

# Early Aptian development and OAE 1a-linked demise of a carbonate platform in the western Tethys: Lower Cretaceous of Sierra Mariola (South Iberian Paleomargin, SE Spain)

Rafael Martínez-Rodríguez<sup>a, b, \*</sup>, José M. Castro<sup>a</sup>, Ginés A. de Gea<sup>a</sup>, Luis M. Nieto<sup>a</sup>, Pedro A. Ruiz-Ortiz<sup>a</sup>, Peter W. Skelton<sup>c</sup>

<sup>a</sup> Dpto. de Geología and CEAETEMA, Universidad Jaén, Campus Universitario, 23071 Jaén, Spain

<sup>b</sup> Dpto. de Paleontología, Estratigrafía y Geodinámica, Universidad Complutense de Madrid, 28040 Madrid, Spain

<sup>c</sup> Independent Researcher, Milton Keynes, UK

## ARTICLE INFO

### Article history:

Received 23 June 2024

Received in revised form

20 October 2024

Accepted in revised form 24 October 2024

Available online 30 October 2024

### Keywords:

Carbonate platforms

Early Aptian

OAE 1a

Paleoclimate

Hothouse events

C-isotopes

## ABSTRACT

A carbonate platform succession of early Aptian age is described from the Sierra Mariola, which is located within the Prebetic Zone of the Betic External Zones (BEZ) of the Southern Iberian Palaeomargin, in SE Spain. The facies and stratigraphic architecture of the studied succession are described and analysed from multiple logged sections to characterize different depositional environments.

The cyclic stacking of facies observed suggests a possible orbital forcing of climate transmitted to sedimentation. Superbundles are recognized describing two sequences of Regressive-Transgressive (R-T) evolution. Analysis of carbon-isotope data identifies both the interval before the hyperthermal event of the early Aptian Oceanic Anoxic Event (OAE 1a) and the onset of the latter event, with an abrupt change in sedimentation marking the demise of the carbonate platform. The field outcrop thus preserves a record of the transition from a greenhouse world to a hothouse event.

© 2024 The Author(s). Published by Elsevier Ltd. This is an open access article under the CC BY license (<http://creativecommons.org/licenses/by/4.0/>).

## 1. Introduction

The episodic growth and demise of carbonate platforms in the Tethys domain during the Aptian are broadly connected to remarkable oceanic, climatic, and biotic changes, within the context of the greenhouse world of the Early Cretaceous (Skelton et al., 2003a; Najarro et al., 2011b; Skelton & Gili, 2012; Hay et al., 2019). Study of the factors that control the development of carbonate successions in the face of eustatic, climatic, and tectonic processes, is necessary for understanding the histories of carbonate platforms (Enos & Moore, 1983; James & Mountjoy, 1983; Eberli & Ginsburg, 1989; Schlager & Philip, 1990; Schlager, 1992; Simo et al., 1993; Rosales, 1999; Graziano, 2000; Wissler et al., 2003; Föllmi et al., 2006; Reijmer, 2021). The Aptian carbonate platforms of the Western Tethys are characterized by a remarkable evolutionary development of rudist bivalves and present transient episodes of orbitolinid-rich facies occurrences. This case study investigates the

complex evolution of a carbonate platform in a rifting geological setting interacting with global and basinal environmental changes, allowing evaluation of the relative roles of the main controlling factors in the sedimentary record (Godet et al., 2011; Huck et al., 2011; Millán et al., 2011; Huck & Heimhofer, 2015).

This work presents a high-resolution stratigraphical and sedimentological study based mostly on four carbonate sections that range from very shallow lagoonal facies to open marine outer platform environments, exposed over a large-scale continuous outcrop. The quality and extent of the outcrops allows correlation of the studied sections and analysis of the evolution of the platform both vertically and laterally. Different facies associations and variable stacking patterns provide a picture of the stratigraphic architecture of the carbonate framework throughout the platform. The facies analysis and their small-scale cyclicity have been the basis for the characterization of a sedimentary model of the platform and analysis of the stratigraphic architecture and the larger scales of cyclicity have been conducted to decipher its sedimentary evolution. Panoramic views across the outcrops reveal the stratal geometries and from the analysis of trends in facies and microfacies we propose a sequence-stratigraphic framework. The integration of

\* Corresponding author. Dpto. de Paleontología, Estratigrafía y Geodinámica, Universidad Complutense de Madrid, 28040 Madrid, Spain

E-mail addresses: [rodrigue@ujaen.es](mailto:rodrigue@ujaen.es), [rafaelma@ucm.es](mailto:rafaelma@ucm.es) (R. Martínez-Rodríguez).

these results within the tectonic, eustatic, and environmental context leads to discussion of the factors that controlled the development of the platform.

Hence this study concerns a shallow-water carbonate platform that was affected by tectonics, biotic crises, and ecological stress at the time of the onset of the early Aptian Oceanic Anoxic Event (OAE 1a), which has been investigated with stable isotope analyses. One specific focus of this work is to obtain clues about how the platform responded to the environmental changes that were particularly associated with the onset of the major carbon cycle perturbation associated with OAE 1a.

## 2. Geological setting

The successions studied in this work encompass the lower part of the lower Aptian (middle to upper members of the Llopis Formation, Castro et al., 2008; Castro, 1998). The study area is situated in the Sierra Mariola (N province of Alicante, SE Spain). This range contains one of the Lower Cretaceous outcrops in the province of Alicante that form part the Internal Prebetic (Fig. 1A) (e.g., Vera, 2004; Vilas et al., 2004; Martín-Chivelet et al., 2019). The Aptian Prebetic platform is also recorded in more internal (proximal)

sectors such as the Sierra de Segura Unit and the Sierra de Bedmar-Jódar Unit (Martínez-Rodríguez et al., 2023). Together with the External Prebetic and the Subbetic, they form the External Zones of the Betic Cordillera, an Alpine Iberian chain. The External Zones of the Betic Cordillera are made of sedimentary units deposited from the Triassic to Early Miocene on the Southern Iberian Palaeomargin (SIP – Fig. 1B), during the Alpine tectonic cycle (Vera, 2001). The development of wide and thick carbonate platforms in the shallow areas of the SIP was favoured by large subsidence rates under an extensional tectonic regime (García-Hernández et al., 2001; García Hernández et al., 2003; Martín-Chivelet et al., 2019) (Fig. 1C).

Basin analysis of the Prebetic platform made by Vilas et al. (1993), allowed the recognition of several tectonosedimentary episodes for the Early Cretaceous. The Aptian represents a main tectonosedimentary episode (K4, Alonso-Chaves et al., 2004) limited by two major discontinuity horizons linked to extensional tectonic events that resulted in significant changes in basin palaeogeography and subsidence patterns. This Aptian tectonosedimentary episode corresponds to a second-order sedimentary cycle in the sense of Hardenbol et al. (1998), which defines a general transgressive-regressive evolution (Castro, 1998; Ruiz-Ortiz & Castro, 1998; Castro et al., 2008).

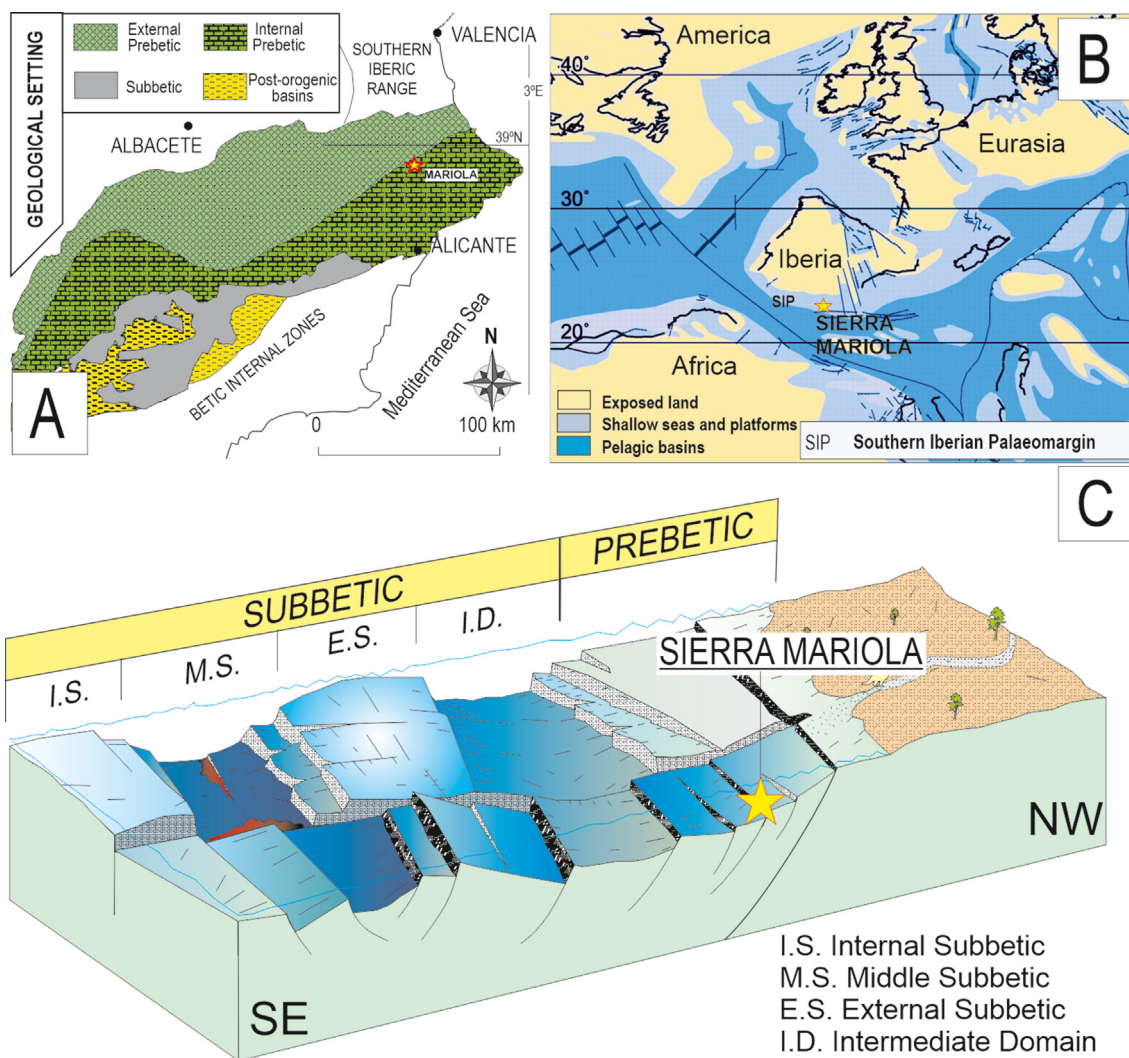


**Fig. 1.** A. Regional geological setting of the Betic External Zones in the E of the Iberian Peninsula (modified from Castro et al., 2008). B. Palaeogeography of the Iberian Plate during the Aptian (simplified from Masse et al., 1993). C. Reconstruction of the tectonosedimentary context for the External Betic Zones during the Early Aptian, modified from Ruiz-Ortiz (2010).

## 2.1. Previous studies on the lower Aptian of Sierra Mariola

The earliest work on the Urgonian facies from the Sierra Mariola was published by Nicklès (1891). Based on that work, Fallo (1943) proposed three different tectonic domains (Betic, Subbetic, and Prebetic Zones). Darder (1945), analyzed the geology of the northern region of Alicante and the south of Valencia, revealing the broad structural, stratigraphic, and palaeontological features. Fallo (1948), made a synthesis of the Betic Cordilleras, concluding that the different tectonic domains previously proposed, had a different stratigraphy and thus, they represent different palaeogeographic domains. Busnardo et al. (1968), studied in detail the Urgonian facies of the Sierra Mariola, with special attention to the ammonoid and orbitolinid faunas. They divided the Urgonian facies into two units, Barremian-lower Aptian, and upper Aptian-lower Albian, separated by a unit of marls with ammonites from the Bedoulian-Gargasian transition. Later studies by Azéma (1971), Company et al. (1982), Granier (1994), and Granier et al. (1995), greatly contributed to the knowledge of biostratigraphy, and to the tectono-sedimentary and the palaeogeographic evolution of the region during the Cretaceous. More recent studies on the lower Aptian of Sierra Mariola include the contributions by Castro (1998), Castro et al. (2008, 2014), Martínez-Rodríguez et al. (2018), and Skelton et al. (2019), made new advances mainly in biostratigraphy, facies relationships, basin analysis, sequence stratigraphy, geochemistry, and their correlation and integration in the global geodynamic and environmental context.

## 3. Material and methods

### 3.1. Lithostratigraphy

The lower Aptian of the Prebetic of Alicante is represented by the Llopis Formation and the Almadich Formation. The Llopis Formation is subdivided into three members (Castro, 1998; Castro et al., 2008) (Fig. 2). This work is focused on the study of the Middle and Upper members of the Llopis Fm. The Lower Member is made of limestones and marlstones, of late Barremian age, and represents a regressive phase (Castro et al., 2008). Over these deposits, the Middle and Upper Member correspond to a new sequence (Castro et al., 2008; Martín-Chivelet et al., 2019). These two members have an early Aptian age: The Middle Member is composed of shallow marine grey limestones with rudists and corals, and the Upper Member (Agres Bed - Fig. 2) comprises bioclastic and sandy limestones, interbedded with marls with orbitolines. The Almadich Fm (early Aptian age) is a rhythmic alternation of marls and marly limestones with ammonites and planktonic fauna, overlying the Llopis Fm (Fig. 2), which was deposited in outer-ramp environments under hemipelagic conditions.

### 3.2. Methods

Four detailed sedimentary logs (410 m in total) recording lithostratigraphy and facies analysis have been carried out, from S to N: La Purísima, Llopis, Racó Llobet and Agres (Figs. 3A-B). The study of sections included sampling for petrographic, microfacies, and biostratigraphic characterization, along with C and O isotopes. The methodology of this study followed classical methods of fieldwork.

In the field, 318 samples were collected from the four studied sections. A total of 318 thin sections were made to describe the petrography and microfacies. The size of the sampling interval was dependent on the thickness of each bed or set of beds, usually selected to document each level, or, in the case of beds thicker than 1 m, to see potential variation between their lower and upper parts.

In intervals with dolomitization, sampling has usually been avoided as dolomitization has erased depositional features. The dolomitization found seems related to burial processes. For diagenetic considerations, the calculated tectonic subsidence (based on the back-stripping method of Bond & Kominz, 1984) of Llopis (Mariola) for the lower Aptian deposits is around 500 m, with a maximum burial depth of 600 m (Castro, 1998).

The study of petrography and microfacies has been made using a stereomicroscope (magnifying glass) LEICA M205C. The Dunham (1962) classification for limestone textures, modified by Embry and Klovan (1971) and monographs by James & Dalrymple (2010), and Flügel (2010), have been used as a reference for facies and microfacies characterization, following standard interpretive and descriptive criteria.

For stable isotope analyses, 130 samples were selected from two of the sections, 15 from La Purísima (distal section) and 115 from Racó Llobet (proximal section). Hard hand samples were carefully micro-drilled to extract the micritic matrix and obtain from it a sedimentary C-isotope signal. To avoid post-depositional features that alter the signal, the sampling zones were delimited with a marker pen over the polished stubs (selected by studying the corresponding thin section), and then sampled using a dental drill (Dremel). Stable isotope measurements were made with a ThermoScientific MAT253 Isotope Ratio Mass Spectrometer connected to a Kiel IV Carbonate Device at the Stable Isotope Laboratory of the Instituto de Geociencias (CSIC, Complutense University of Madrid).  $\delta^{13}\text{C}$  and  $\delta^{18}\text{O}$  values of the carbonate were calibrated against certified carbonate standards (NBS-19). All the isotope data are reported in per mil (‰) versus Vienna-Pee Dee Belemnite (V-PDB) standard. The analytical precision of repeated standard measurements is always better than 0.025 ‰ for both carbon and oxygen (Supplement).

The four sections presented are a compilation of different outcrop observations and analyses, using the correlation of characteristic beds from panoramic outcrop pictures to make direct physical correlation possible. Helicopter aerial views taken in 2007, provided by J.M. Castro, have been used to generate large panoramic compound images, to adjust precision for the stratigraphic correlation, and to analyze the geometric disposition of strata packets to refine the stratigraphic architectural framework based on the study of the outcrops.

## 4. Results

### 4.1. Stratigraphy summary

La Purísima section (Fig. 3A, WGS84 coordinates: bottom 38°44'56.37"N 0°27'49.72"W; top 38° 44'59.208"N 0°28'18.751"W) is 159 m thick and is composed of limestones with less abundant intercalated marly levels. This section shows marked vertical facies changes between grainstones, floatstones/rudstones with corals and rudists, and mudstones (see Fig. 4). The location of the Llopis section (Fig. 3A) is to the South of the "Balcón de Llopis", a steep wall in the center of the East side of Sierra Mariola (WGS84 coordinates: 38°45'27.7"N 0°28'45.7" W) (Fig. 3B). The Llopis section is 53 m thick (Fig. 4), and its position is key to connecting distal (outer) and proximal (inner) environments of the Aptian carbonate platform and contains the upper part of the Llopis clinofolds where the carbonate beds present progradational geometries southwards (Skelton et al., 2019). The Racó Llobet section (Fig. 3B) WGS84 coordinates are bottom; 38°46'3.60" N; 0°29'33.5544" W; top: 38° 45' 51.53148" N; 0°29'32.559" W. The section is 118 m thick (Fig. 4). The first 38 m are characterized by the presence of limestones and grainstones with corals. The middle part consists of nodular and often bioturbated marly limestones. Its lower part

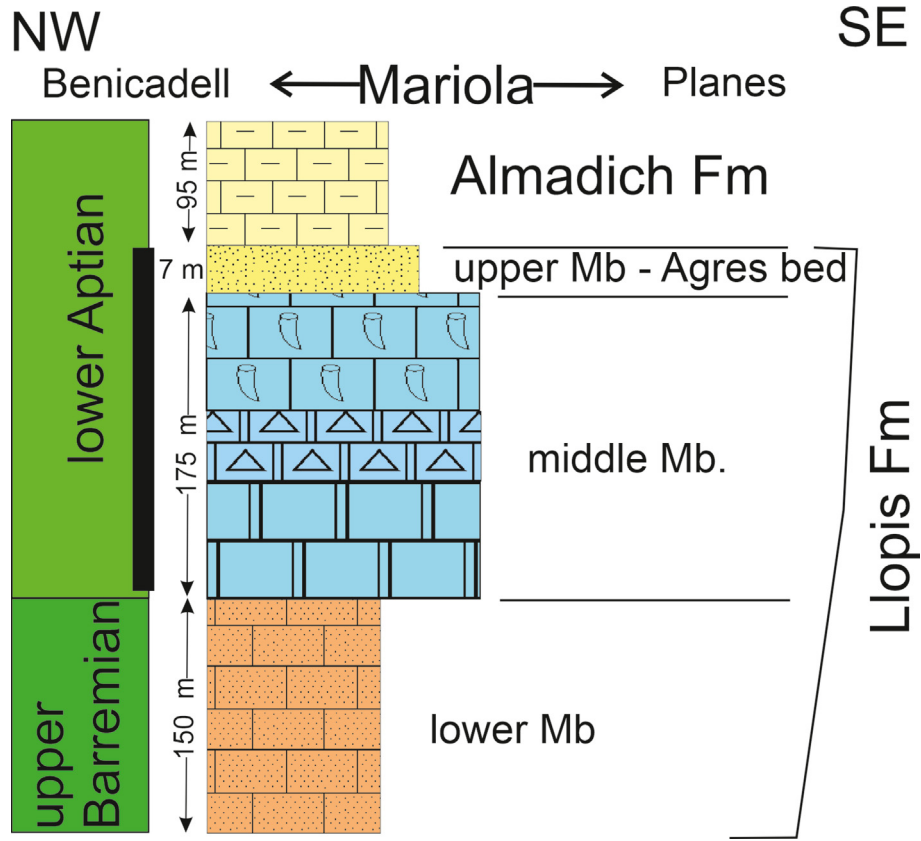


Fig. 2. Lithostratigraphic scheme of the upper Barremian-lower Aptian (p.p.) in the Sierra Mariola (Alicante, Spain). The black vertical bar represents the materials of this study.

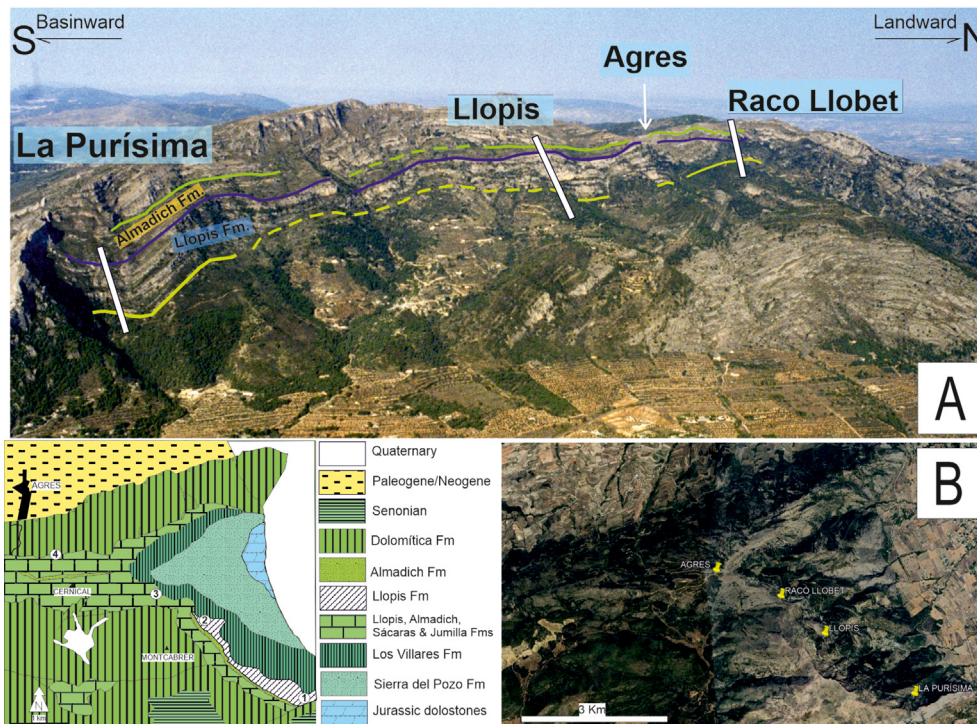
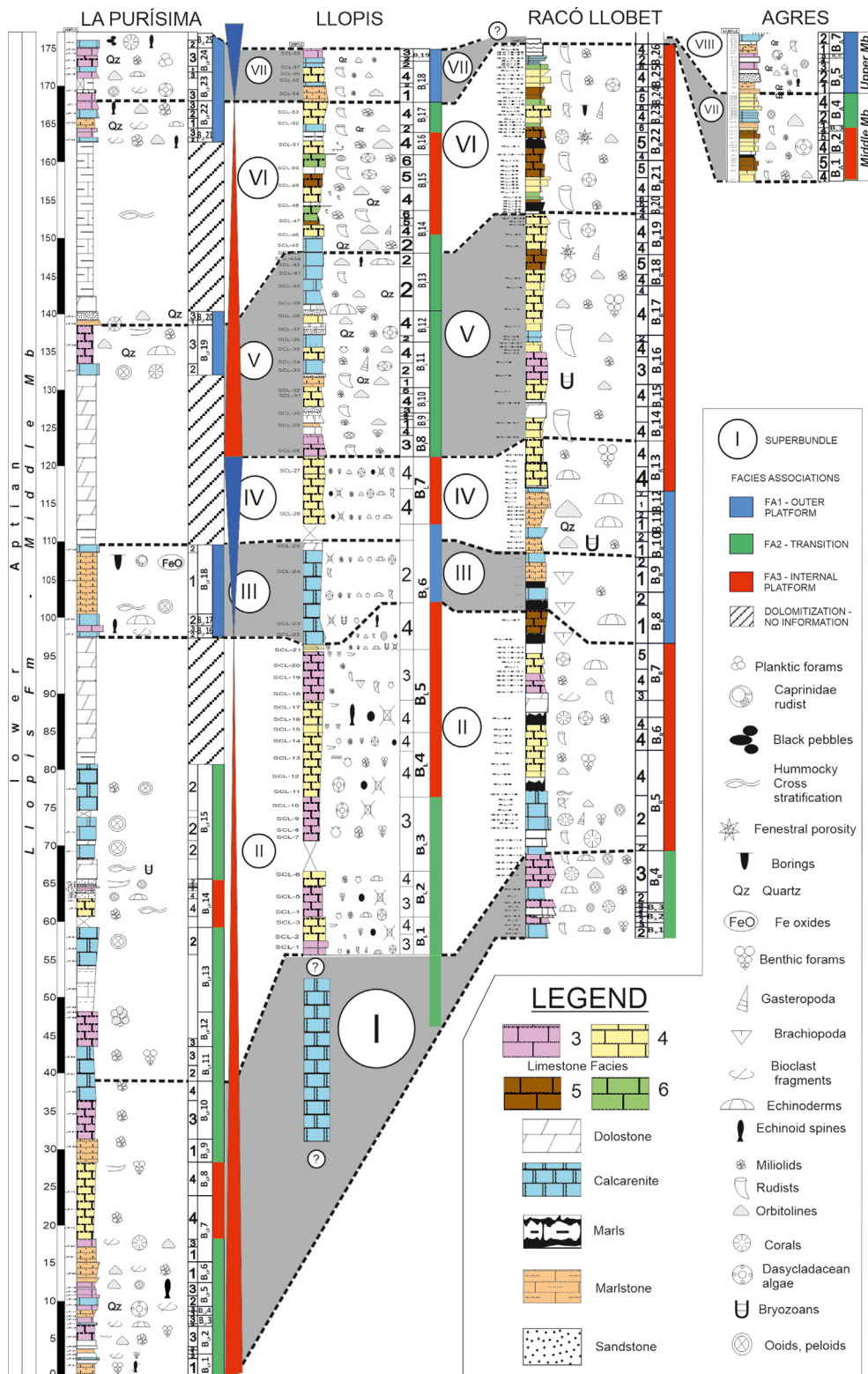


Fig. 3. A. Aerial view of eastern slope of Sierra Mariola, studied in this paper. Drawn lines highlight Llopis and Almadich formations, the location of the four sections studied in this work are indicated. B. Left: Geological map of Sierra Mariola. Modified from Castro (1998). Right: Satellite image of Sierra Mariola. The position of the sections studied is indicated. 1: La Purísima; 2: Llopis; 3: Racó Llobet; 4: Agres.



**Fig. 4.** Correlation scheme for the studied sections. From left to right, the four stratigraphic columns are: La Purísima, Llopis, Racó Llobet, and Agres. Facies types are indicated with roman numbers, bundles are indicated as upside arrows, superbundles are indicated with roman numbers. Regressive-Transgressive trends are indicated with a red and blue arrow, respectively.

(from 38 to 50 m) contains abundant brachiopods, whereas the upper part of this middle part (from 50 to 60 m) is rich in orbitolines. The upper part, from 60 to 118 m, is composed mainly of well-bedded limestones with rudists. The Agres section is 18 m

thick (Fig. 4). This section is located on the northern face of Sierra Mariola (Fig. 3A-B). Its position is the most proximal of the four, and it was selected to study the transition from the Middle Member of the Formation to the Upper Member of the Formation, the

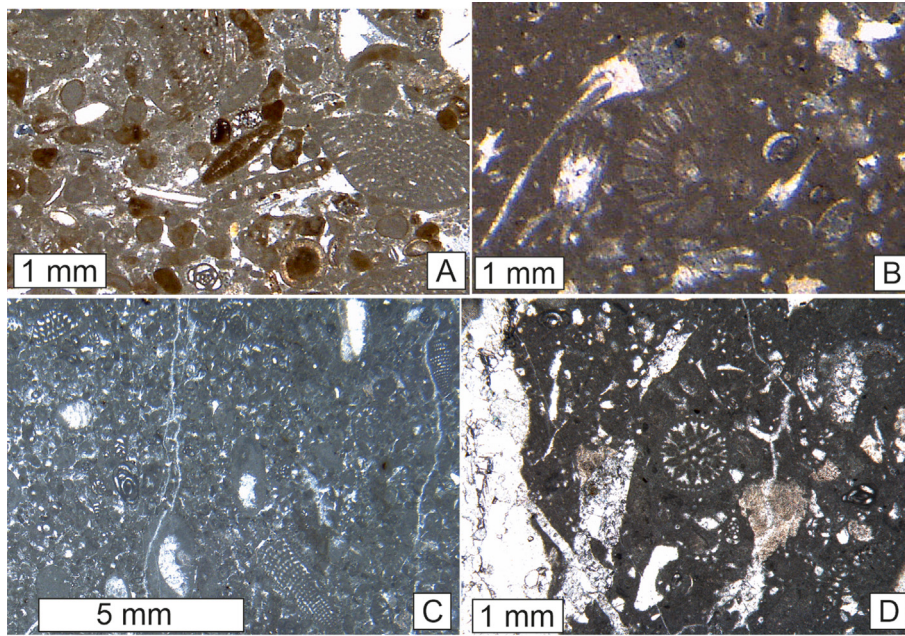


**Fig. 5.** Photomicrographs: A. Sample SCL-14, showing *Orbitolinopsis buccifer*, *Paracoskinolina maincy* and *O. praesimplex*. B. Detail of *Orbitolinopsis praesimplex* (sample SCL-9). C. Axial section of *Choffatella decipiens* (sample SCL-23). D. Oblique subequatorial section of *Choffatella decipiens* (sample LA-2).

Agres Bed. This Upper Member displays an enrichment in quartz content and shows a very particular microfacies association of conical and planar orbitolinids, with abundant transported recumbent-type rudists (Caprinidae) (Skelton et al., 2019). The top of this member is a planar surface with borings and encrusted ostreids that represent a firmground formed during the interruption of the platform sedimentation (Skelton et al., 2019).

4.2. Biostratigraphy – age constraints

Caprinid rudists *Offneria interrupta* have been found at the base of the Racó Llobet section, and *Caprina douvillei* at the top (Skelton et al., 2019). The lower part of La Purísima section has *Sabaudia* sp., *Derventina* sp., and *Choffatella decipiens* (Fig. 5A-B) benthonic foraminifera. Also, orbitoline *Paracoskinolina maynci* has been found at the lower part of La Purísima. Other orbitolinids found are *Orbitolinopsis kiliani*, *Orbitolinopsis buccifer* (Fig. 5C), and

*Orbitolinopsis cuvillieri*, the presence of the last one in this association is indicative of the uppermost Barremian to lowermost Aptian (*Martelites sarasini*-*Deshayesites ogranlensis* zones, Bonvallet et al., 2019). Planktonic foraminifera *Hedbergella sigali* has been recovered in the middle part of the Racó Llobet section. Collectively, these data indicate an early Aptian (early Bedoulian) age, which is consistent with previous data (e.g., Busnardo et al., 1968; Company et al., 1982; Castro et al., 2008; 2014; Skelton et al., 2019). Associations of orbitolinids have permitted the recognition of two biostratigraphic units (Castro et al., 2001): one with *O. killiani* and *O. cuvillieri*, recorded in the lower part, and the other with *Orbitolinopsis praesimplex* (Fig. 5D), whose first record occurs at the middle part of the unit.

Consequently, the time interval represented by the studied succession is correlated with the following planktonic foraminifera and ammonite biozones (Castro et al., 2001; Martín-Chivelet et al., 2019) (see Fig. 6):

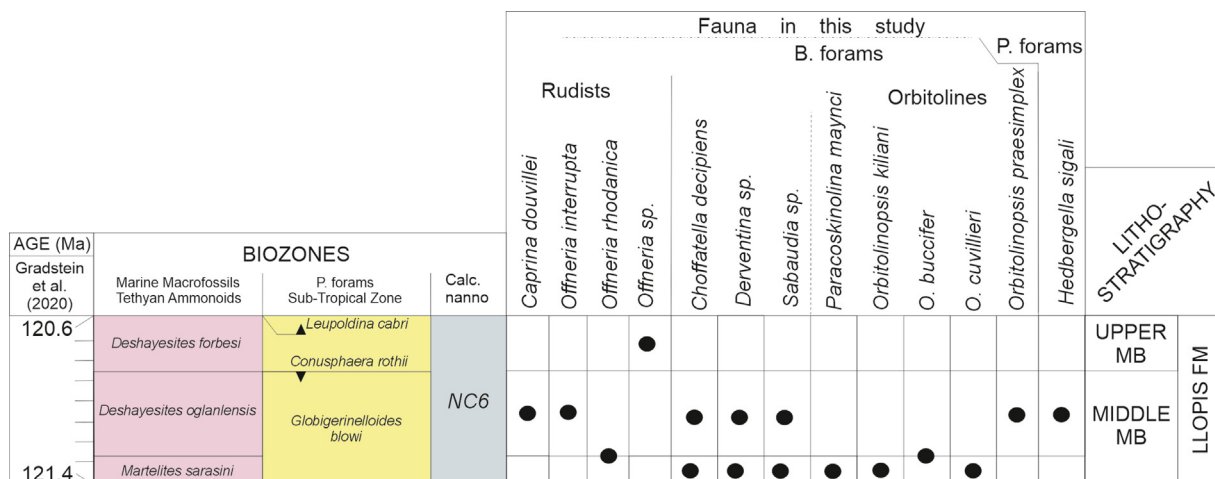


**Fig. 6.** Biostratigraphic chart for the studied materials. Time scales of Gradstein et al. (2020) is shown on the left.

**Table 1**  
Lithofacies, facies associations and environmental interpretation of the studied materials.

Facies	F.A.	Lithofacies description	Environmental interpretation
1	Facies Association 1	1a: Packstone and wackestone almost entirely composed of orbitolinids (orbitolinite), mostly planar, and with small bioclasts and planktic foraminifera. Less common grains are brachiopods, cortoids, crinoids, scarce rudist fragments, bryozoans and gastropods. The matrix is a peloidal micrite with fine quartz grains.	Circalittoral. Open/outer platform. Open marine environments with moderate to low energy.
2		Bioclastic grainstones with 1 mm mean sized grains and sparry cement. Grains are coated bioclasts, exhibit micrite envelopes or are completely micritized. It contains intraclasts, micritized grains, peloids, ooids, cortoids, and some bioclasts such as molluscs, red algae, echinoid spines, crinoids and benthic foraminifera. Some grains contain Fe-oxide. The intraclasts are poorly-sorted and sub-angular to sub-rounded in shape.	Circalittoral/infralittoral. Platform margin banks, in a shallow marine subtidal context with moderate energy.
3	Facies Association 2	Grey limestones and marlstones with scleractinian corals, with wackestone to packstone texture. The corals are small (cm-size) irregular bioclasts often encrusted by red algae, with micrite coatings and borings filled with sediment. The matrix presents bioclasts and benthic foraminifera (mostly miliolids and orbitolinids), along with some lime mudstone intraclasts intensely burrowed.	Infralittoral. Build-ups forming reef patches or scattered coral colonies, in the convergence between the outer and the inner platform, under moderate energy, sometimes affected by storms.
4	Facies Association 3	Floatstones and packstones with rudists, along with <i>Chondrodonta</i> , other bivalves, coral fragments, and another vagile organisms like echinoderms and gastropods. The matrix is a bioclastic wackestone (locally packstone), with small skeletal debris, including benthic foraminifera (miliolids and orbitolinids with conical morphology), and dasycladacean algae.	Lagoon environment of the inner platform. Low energy, external lagoon, with moderate water circulation.
5		Wackestones and packstones with abundant miliolids and orbitolinids, among other planispiral, trochospiral and biserial benthonic foraminifera.	Infralittoral. Shallow subtidal low-energy environment corresponding to the internal part of the inner platform.
6		Mudstones with scarce small miliolids and undifferentiated bioclasts. The micrite displays small (mm-size) fenestral pores.	Very shallow low-energy environment with restricted circulation. The fenestral porosity indicates a tidal environment (foreshore).
Facies 7		Bioclastic and sandy (up to 50% quartz) limestones with packstone texture, displaying caprinid rudists, orbitolinids, and with benthic foraminifera, miliolids, dasycladacean algae, peloids and brachiopods.	Outer/margin platform environment.

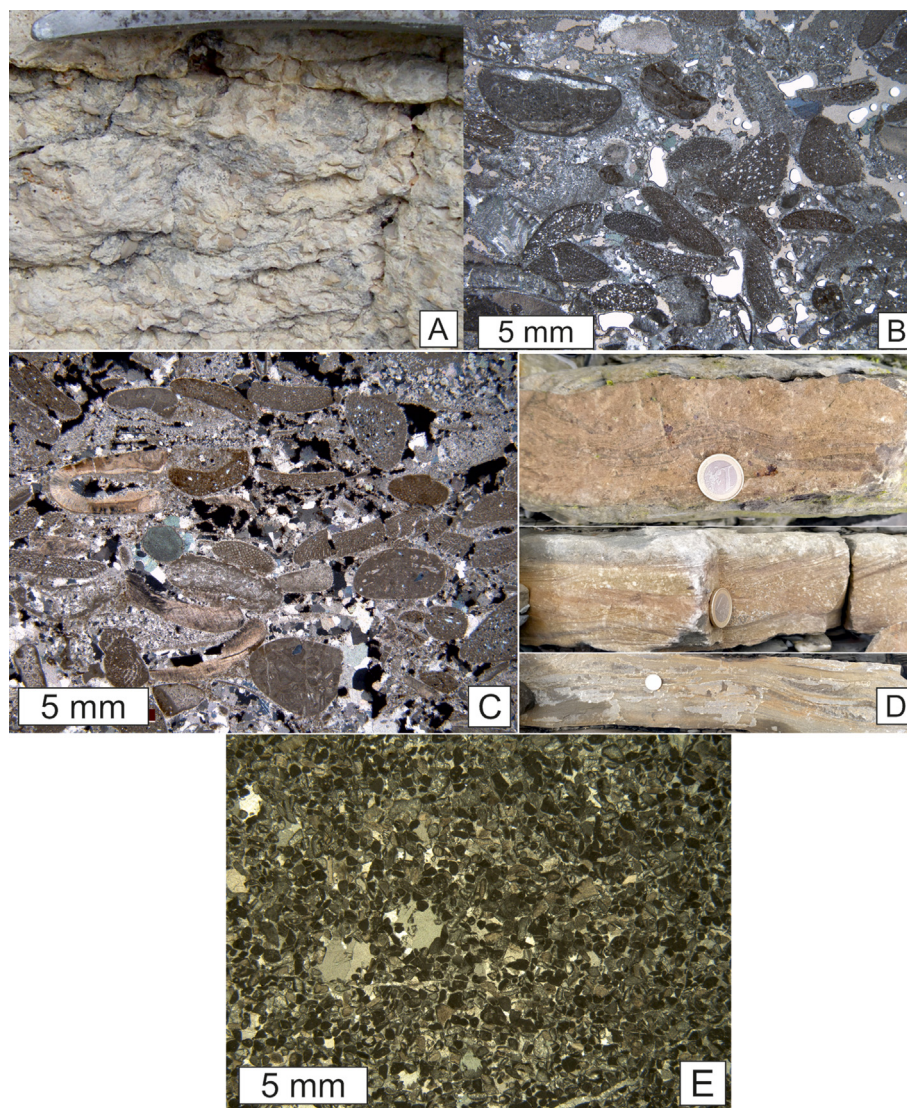


**Fig. 7.** A. Orbitolinite facies. B–C. Microfacies Type 1a “orbitolinite” facies. In these samples showing sparry cemented matrix with accumulation of bioclasts, mostly planar orbitolines, parallel-oriented. C-D. Field examples of cross stratification (hummocky) found in La Purísima section. E. Grainstone texture of calcarenitic facies type 2.

- The base of the studied platform corresponds to the uppermost part of *M. sarasini* ammonite zone (part lacking *O. praesimplex*). The middle part of the studied platform corresponds to the *D. oglanlensis* ammonite zone (part with *O. praesimplex*). Collectively, the Middle Mb of the Llopis Fm corresponds to the upper part of the *Globigerinelloides blowi* biozone of planktonic foraminifera and to the upper part of the NC6 biozone of calcareous nannofossils. At the top of the studied platform, the Upper Mb corresponds to the lower part of the *Deshayesites forbesi* ammonite zone (Gradstein et al., 2020). The Upper Mb (Agres Bed) is a horizon placed between the LO of the calcareous nannofossil *Conusphaera rothii* and the FO of the planktonic foraminifera *Leupoldina cabri* (Castro et al., 2021). This level coincides with the negative excursion that marks the onset of OAE 1a (Skelton et al., 2019).

#### 4.3. Sedimentology

##### 4.3.1. Facies analysis

The combined field and microfacies detailed study have led to the differentiation of seven main facies types (see Table 1 and Figs. 7 and 8); Facies 1 to 6 correspond to a depositional model of

the platform whereas Facies 7 corresponds to a different sedimentary context within the platform. The interpretation of the character of each facies has been made following classic literature (Bathurst, 1975; Wilson, 1975; Tucker & Wright, 1990; Flügel, 2010).

- **Facies 1** (Fig. 7A-B-C) – **Description:** packstones and wackestones almost entirely composed of orbitolinids (orbitolinite). The matrix is a micrite with peloids and fine quartz grains, and it also contains small skeletal fragments of such as echinoids and planktic foraminifera. The orbitolinids are mostly planar or discoidal. Less common grains are brachiopods, cortoids, crinoids, scarce rudist fragments, bryozoans, and gastropods.

**Interpretation:** These facies have a circalittoral character and represent the outer or open marine platform (Arnaud-Vanneau, 2005; Stein et al., 2012). The abundance of quartz and relative lack of muddy micrite suggests a moderate to low hydrodynamic level, indicating an offshore-transition or lower shoreface, in the limit of the storm wave base (Pemberton et al., 2012).

- **Facies 2** (Fig. 7D-E-F) – **Description:** is represented mainly by medium to coarse, poorly sorted brownish grey grainstones which are arranged in metre-thick beds with local, small-scale cross-stratification and sometimes hummocky cross-stratification

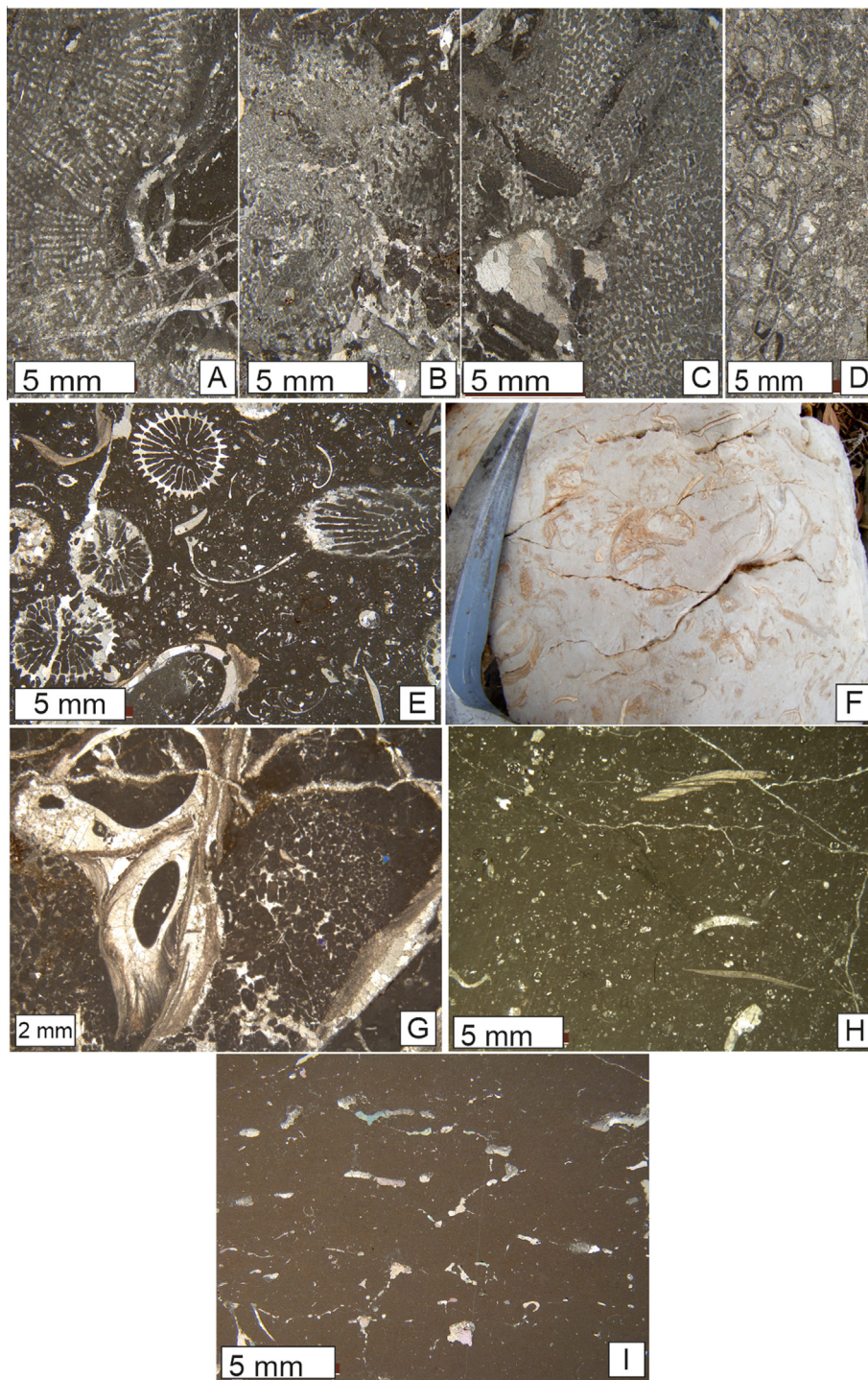


**Fig. 8.** A-B-C-D. Coral facies type 3. E. Facies 3 with wk matrix showing solitary corals. F-G. Rudist facies type 4 showing rudist floatstone lithofacies (F) and microfacies (G). H. Facies type 5 wackestone with miliolids and other benthic foraminifera. I. Facies type 6, mudstone with fenestral porosity.

(Fig. 7D). The microfacies are bioclastic grainstones with sparry cement (Fig. 7E). Grains are mostly coated, in some cases by a micritic penetrative rim, appearing completely micritized. They are intraclasts, peloids, ooids, cortoids, and some bioclasts such as molluscs, red algae, echinoid spines, crinoids, and benthic foraminifera. Some grains contain Fe-oxide. The intraclasts are poorly sorted and sub-angular to sub-rounded in shape.

**Interpretation:** Circalittoral/infralittoral location. These facies record relatively moderate current energy background conditions, with occasional storm disturbance (producing the hummocky

cross-stratification); the relatively unrounded shape does not suggest a very intense winnowing (Kidwell et al., 1991). These facies are subjected constantly to moderate hydrodynamics (e.g. shoreface or deposition between fair- and storm-wave base) and develop in shallow subtidal environments (Arnaud-Vanneau, 2005). The cross-stratification indicates that currents acted continuously on the substrate (Giannetti et al., 2014).

- **Facies 3** (Fig. 8A-B-C-D-E) – **Description:** grey limestones and marlstones with fragments of scleractinian corals, usually with wackestone to packstone matrix texture. The corals are small (cm-

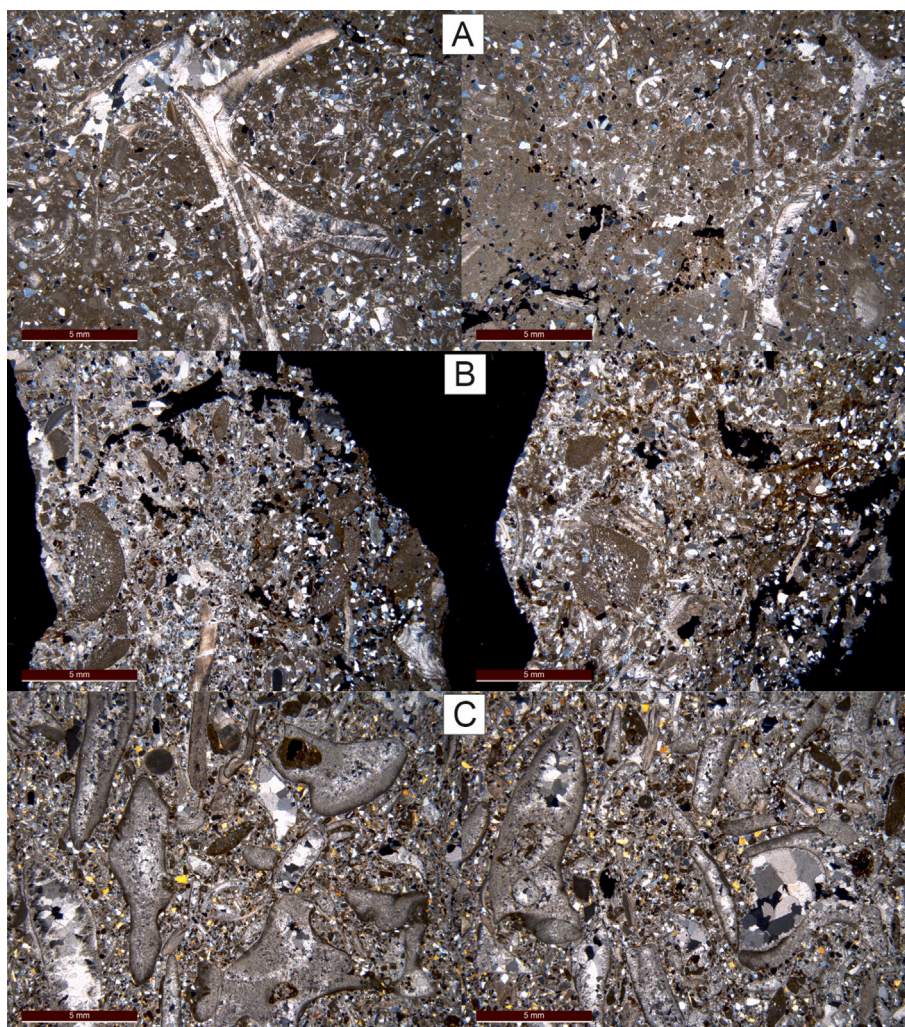


**Fig. 9.** Facies type 7. Microfacies from the Superbundle VIII in the Agres section. Sandy packstone texture with quartz grains up to 50 %. Different fauna association shown. A. With requieniid rudists. B. With planar and conical orbitolines. C. Larger bioclasts (mollusks) rich-bearing facies with extensive and pervasive diagenetic cement showing the replacement of ex-aragonitic shells by calcite.

size) irregular bioclasts, and tubular solitary specimens, often encrusted by red algae, with micrite coatings and borings filled with sediment. The matrix presents bioclasts and benthic foraminifera (mostly miliolids and orbitolinids), along with some lime mudstone intraclasts, and is intensely burrowed.

**Interpretation:** This facies type is interpreted as derived from coral patch reefs (Armella et al., 2008) or scattered coral colonies in a protected backshoal setting (Beresi et al., 2017). The abundance of micrite and preservation of fauna suggest a moderate to low hydrodynamic level. As the corals are not found in a life position, proper boundstone lithofacies are not observed in the field, so it is difficult to explain the facies as a complete coral rim barrier system. The presence of marlstones suggests some terrigenous input, instead of the classic nutrient limitation model applied for most present-day coral reefs (with well-illuminated and oligotrophic waters); these corals developed in turbid and mesotrophic waters, thus their presence does not imply an important carbonate production (Löser, 2001; Tomás et al., 2008). Collectively, these facies present an infralittoral character in the transition (middle part) of the platform, with

occasional storm events affecting depositional processes (Stein et al., 2012).

- **Facies 4 (Fig. 8F-G) – Description:** corresponds to floatstones and packstones with rudists, along with *Chondrodonta*, other bivalves, coral fragments, and vagile organisms like echinoderms and gastropods. The matrix is a bioclastic wackestone (locally packstone), with small skeletal debris, including benthic foraminifera (miliolids and orbitolinids with conical morphology), and dasycladacean algae.

**Interpretation:** These facies were deposited in shallow environments with low energy and moderate water circulation in lagoon environments and related to the external part of the inner platform (“external lagoon” facies) (Arnaud-Vanneau, 2005).

- **Facies 5 (Fig. 8H) – Description:** is represented by wackestones and packstones with abundant benthic foraminifera, such as miliolids and orbitolinids, among other planispiral, trochospiral and biserial benthonic foraminifera.

**Interpretation:** These facies represent a relatively calm, infralittoral environment (shallow subtidal), and correspond to inner platform environments (internal part of the inner platform) (Stein et al., 2012).

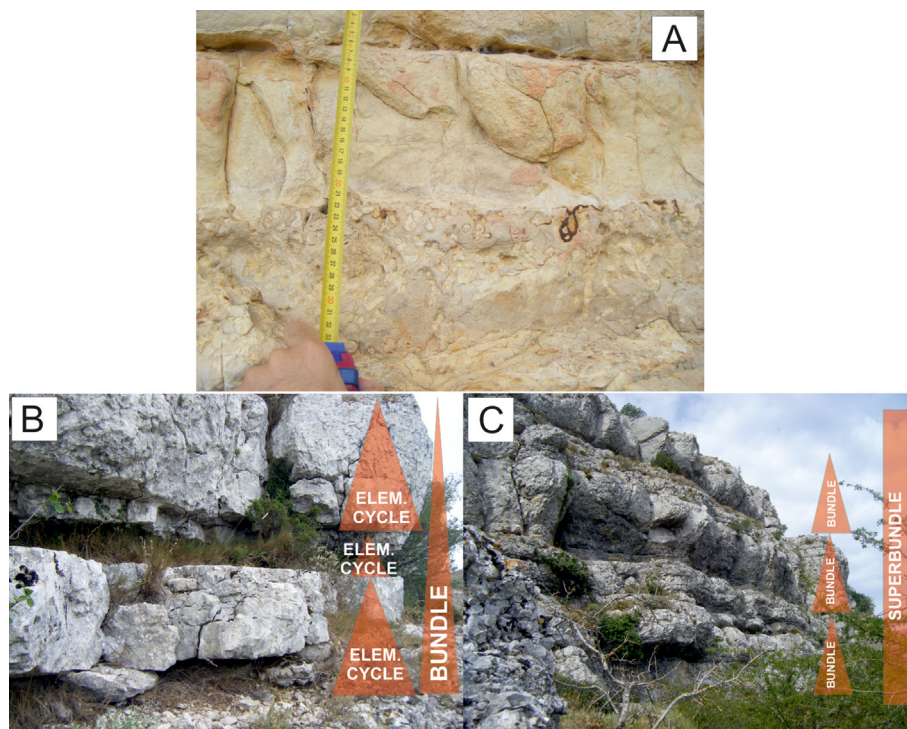


**Fig. 10.** Field photographs from Sierra Mariola. A. Hiatus (hardground) with Fe-iron crust and borings developed on the stratigraphic horizon. B–C. Stratigraphy units defined in the study as elementary cycles (6th order), bundles (5th order) and superbundles (4th order).

- **Facies 6** (Fig. 8I) – **Description:** is represented by mudstones with scarce small miliolids and undifferentiated bioclasts. The micrite displays small (mm-size) fenestral pores. The size of the micropores is heterogeneous, with some up to 5 mm long and 1 mm wide, and smaller ones that are 0.5 mm wide and 2–5 mm long. The effective porosity is low due to the poor interconnection of the pores, usually separated by 1–5 mm of matrix.

**Interpretation:** These facies are interpreted to be deposited under very shallow, low energy environments. The fenestral porosity indicates a tidal environment (e. g. foreshore) (Photiades et al., 2010). The lack of echinoderms is suggestive of restricted circulation (Arnaud-Vanneau, 2005).

- **Facies 7** (Figs. 9A-B-C) – **Description:** Bioclastic limestones and mixed siliciclastic limestones. It presents a packstone texture, with quartz sometimes present up to 50 %, requieniid rudists (Fig. 9A), planar and conical orbitolinids (Fig. 9B), and irregularly shaped bioclasts partially leached and cement-filled ex-aragonitic shell (Fig. 9C) of indeterminate molluscan origin. It also presents benthic foraminifera, miliolids, rudist fragments, dasycladacean algae, peloids and brachiopods. These facies are restricted to the Upper Mb of the Llopiis Fm.

**Interpretation:** outer/margin platform depositional environment, based on the presence of redeposited caprinid rudists and the abundance planar orbitolines (Gili & Götzt, 2018).

#### 4.3.2. Elementary cycles and facies associations

The described facies are stacked in metre-scale elementary cycles, which can be classified into three overlapping vertical associations of facies (FA1, FA2, and FA3). By application of Walther's law, these vertical associations of facies generally follow a 1-2-3-4-5-6 (Facies 7 belongs to another context), reflecting the lateral facies relationships during deposition (Fig. 10), though with some omissions and reversals. The first facies association (FA1, facies

1–2) is largely composed of packstones with orbitolinids, wackestone/packstone with brachiopods, and marlstones with corals, present in the middle part of the sections (Fig. 4; metres 97.5 to 120–122.5). The second facies association (FA2, facies 2 to 3) is represented by successions starting with bioclastic-skeletal calcarenites (grainstone-packstone) followed by limestones (locally wackestones) with corals, and it is mainly present in the lower part of the sections (Fig. 4; from 0 m to 100 m). The third facies association (FA3, facies 4-5-6) is composed of calcarenites, rudist floatstones, and wackestones or mudstones with burrowed or bored tops, and dominates the upper part of the sections (Fig. 4; between 110 and 170 m). The presence of peloids and red algae in facies 2 indicates an open marine influence, whereas the tubular solitary corals in facies 3 indicate a shallower character. Thicker beds found in this study indicate that carbonate productivity was high enough to fill the relatively high accommodation space, while parts with thinner cycles suggest a decrease in accommodation space.

In general, these facies associations are interpreted as shallowing-upward cycles. FA 2 represents repeated platform-top cycles, stacked within an overall aggradational trend: the main influence on the change in facies in each cycle would have been the frictional attenuation of current strengths, hence circulation, with increasing distance from the outer margin of the platform top.

#### 4.3.3. Cyclicity

Collectively, the analysis of cyclicity reveals three orders, from smaller to larger scale (6th, 5th, and 4th order), named here as elementary cycles (6th order), bundles (B - 5th order), and superbundles (SB - 4th order). The succession of facies recorded in each elementary cycle is deposited under continuous sedimentation, with gradual changes in the sedimentary conditions.

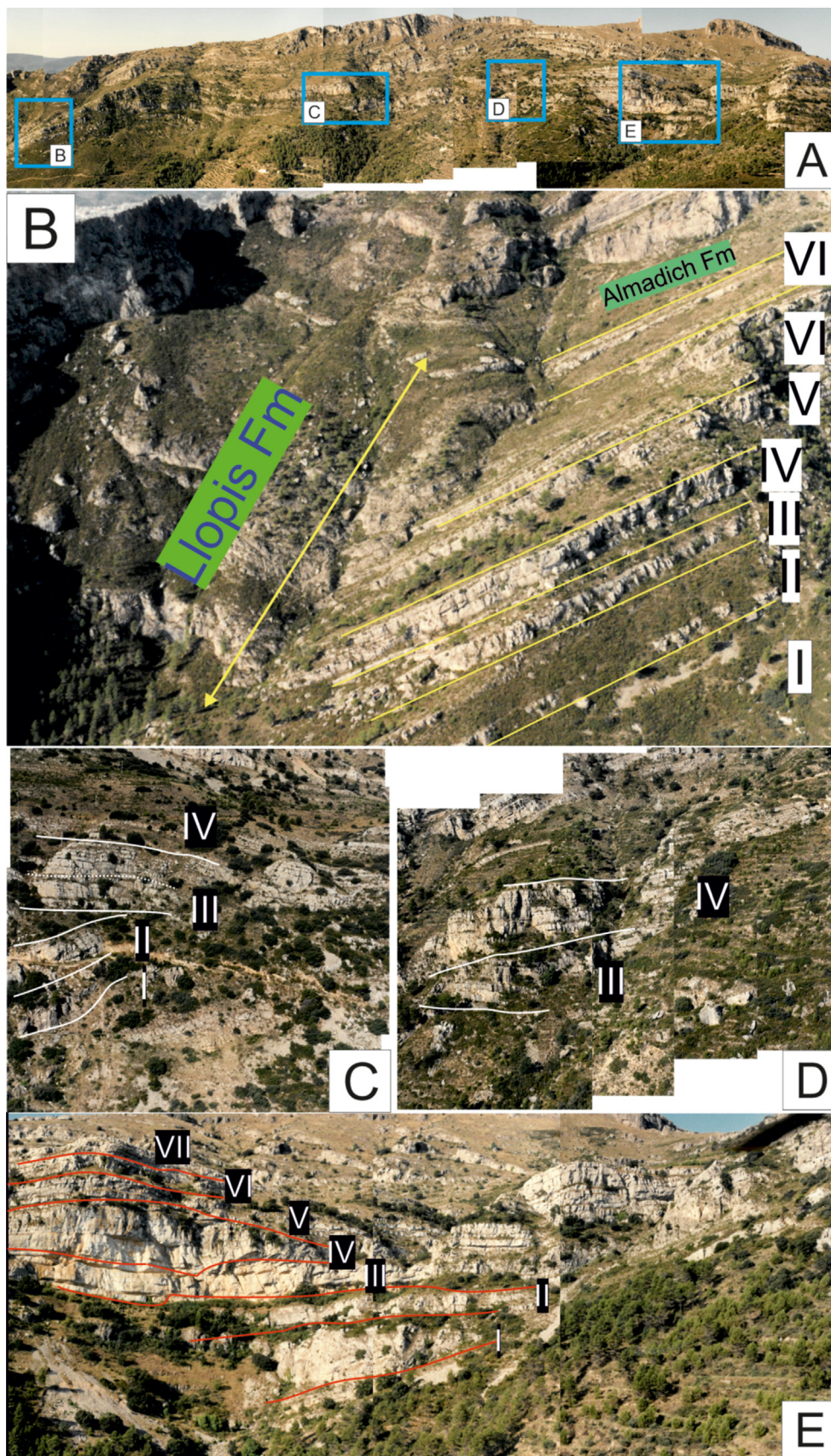


**Fig. 11.** Images from La Purísima section taken from helicopter flight, in which the superbundles of the Middle Mb of the Llopis Fm can be seen, separated by lines, and indicated by numbers. A. Aerial view of the Eastern slope of Sierra Mariola, B–C–D–E indicate outcrop positions referred following this figure. B. Superbundles of the middle member of the Llopis Formation at La Purísima section. The location can be seen in Fig. 11A. C. Stratigraphic relations between superbundles I and II, dipping SW, while III and IV are horizontal. These outcrops are located close to the Llopis section. D. Stratigraphic relations between superbundles III and IV in the Llopis section area. E. Stratigraphic relations between superbundles I, II, III, IV, V, VI and VII, close to the Racó Llobet section.

One of the most pervasive characteristics of the studied succession is the vertical cyclicity defined by the stacking pattern of the elementary cycles of facies. These elementary cycles are limited by neat surfaces, considered to represent sharp changes in the sedimentary conditions, likely hiatuses, especially when features such as iron crusts or borings appear on these surfaces (Fig. 10A). The elementary cycles constitute the most elemental order of cyclicity (6th order) (Fig. 10B). These metre-scale elementary cycles are considered the basic unit of shallow-marine carbonate platforms (Evans et al., 1977; Grotzinger, 1986; Hardie et al., 1986; Einsele et al., 1991; Demicco & Hardie, 1995; Elrick, 1995; Satterley, 1996; Bosence et al., 1999; Immenhauser & Scott, 2002; Pittet et al., 2002; Sandulli & Raspini, 2004). The analysis of facies and their associations permits the determination of bundles across the sections, which constitute the next hierarchical order of cyclicity (5th order) (Fig. 10B). Bundles have been defined here as sets of beds that begin with a determined type of facies, and together with field observations and petrography analysis, they describe a complete succession that generally goes from deeper or distal facies to shallower or proximal facies. On a larger scale, these bundles can be seen in the field and on aerial images as packs that are laterally continuous through the outcrops, defined as superbundles (SB) (Fig. 10C). Up to eight superbundles (described in 4.3.4) have been defined, constituting the 4th order of hierarchy in cyclicity.

In the La Purísima section, at least 25 bundles ( $B_{LP1}$  to  $B_{LP25}$ ; Fig. 4) have been recognized; nevertheless, due to dolomitization, it is difficult to observe the original sedimentary features at some parts of the section, where more bundles are probably present. The thickness of the bundles is variable between 1 and 2 m thick (Fig. 4; bundles  $B_{LP3}$ , 4, 16, 17, 20, 21 and 25) and 10–15 m thick (Fig. 4;  $B_{LP7}$ , 10, 13, 15 and 18). In the Llopis section, 19 bundles ( $B_L1$  to  $B_L19$ ) have been recognized. The bundles are thicker in the lower part of the section (Fig. 4; superbundles II to IV; from 55 m to 120 m), with 7 bundles ( $B_L1$  to  $B_L7$ ) displaying a thickness from 5 to 15 m. In the upper part of the section (Fig. 4; superbundles V to VII; metres 120 to 175), the bundles ( $B_L8$  to  $B_L19$ ) are generally thinner, no more than 10 m thick. The Racó Llobet section shows 26 bundles ( $B_R1$  to  $B_R26$ ) that have different thicknesses between 2 and 3 m to more than 10 m. The lower four bundles belong to superbundle I (SB I), and the following three make the superbundle II (SB II). Superbundle III is formed by 2 bundles. 13 bundles have been recognized in the upper part of Racó Llobet section. The 4 bundles of the superbundle IV (SB IV), are, in general, thicker (5–7 m) than the 6 bundles of superbundle V (SB V), which are generally organized in packages of 2–3 m, in a thinning-upward trend. Superbundle VI (SB VI) presents 7 bundles (Fig. 4;  $B_R20$  to  $B_R26$ ), from 152.5 to 175 m. Only the base of superbundle VII is well exposed in this section. The Agres section has 7 cycle-bundles ( $B_A1$  to  $B_A7$ ) (Fig. 4). The first 4 bundles are part of the superbundle VII (SB VII), while the 3 upper bundles are part of the Agres Bed (or superbundle VIII – SB VIII) (Fig. 4).

#### 4.3.4. Stratigraphic architecture

One of the key aspects of the Middle Member of the Llopis Formation at Sierra Mariola is its great lateral continuity, constituting an almost continuous outcrop, although the Upper Member is only present in the Agres section. The eastern slope of the range offers a large-scale natural NNE–SSW cross-section cutting the carbonates through 1650 m. The lateral correlation of sections has been made by taking reference horizons such as marly levels or ferruginous surfaces, with the help of aerial views and helicopter images (Fig. 11A). This allowed the subdivision of the Middle Member into seven superbundles (sequences I to VII shown in

Figure 11B). These superbundles can be seen in the panoramic views from the outcrops and are recognized in the cyclicity analysis of each studied section. To correlate the superbundles, we have integrated strata morphology data obtained from the field with the analysis of aerial photography.

##### Superbundle I – SB I

The first superbundle crops out in the lowermost part of La Purísima and Racó Llobet sections, with a thickness of 15 and 12 m, respectively. It has been recognized below the Llopis section, although the outcrop conditions hampered detailed logging. The base is delimited by bundles  $B_{LP1}$  at La Purísima and  $B_R1$  at Racó Llobet (Fig. 4).  $B_{LP1}$  is 3 m thick and presents benthic forams and fragments of echinoid spines, whereas  $B_R1$  is 2 m thick and presents an association of facies 2 and 3, with ooids, benthic forams, echinoderms, and rudists. In general, this superbundle is formed by grey calcarenites showing small-scale cross-stratification and grainstone microfacies with crinoids, brachiopods, and small benthic foraminifera (FA 2). Some internal facies (FA 1) are intercalated at La Purísima section within bundles  $B_{LP7}$  and  $B_{LP8}$  but affected by dolomitization (Fig. 4). The top is delimited by bundle  $B_{LP10}$  at La Purísima, which is 7.5 m thick and presents an association of facies 3 and 4, while at Racó Llobet the top is formed by  $B_R4$ , with 6 m of thickness and an association of facies 2 and 3.

##### Superbundle II – SB II

This superbundle is present in La Purísima, Llopis and, Racó Llobet sections. The thickness in La Purísima is 60 m, 40 m in Llopis, whereas in Racó Llobet it is 30 m. The predominant facies are grey to white limestones with macrofossils (rudists and *Chondrodonta*) (facies 4). This pack of strata is aggradational, presenting clinoforms at the Llopis section, which give it a sigmoidal shape showing incipient progradational morphology (Fig. 11C). Facies change laterally from packstone with corals at Racó Llobet (proximal environment) to skeletal grainstones at La Purísima (distal environment) (Fig. 4). The lateral facies change is recorded in the Llopis section.

##### Superbundle III – SB III

Superbundle III is present at La Purísima, Llopis, and Racó Llobet sections. This superbundle is 10 m thick at Racó Llobet, passing to 15 m at Llopis and 13 m at La Purísima. This superbundle is composed of aggradational beds with outer platform facies (FA 1) in La Purísima, Racó Llobet and Llopis sections.

##### Superbundle IV – SB IV

This superbundle is 15 m thick at Racó Llobet, and 11 m thick at Llopis, passing to 12 m at La Purísima. It contains parallel strata (Fig. 11D) with nodular levels with planar orbitolinids and echinoids in Racó Llobet and Llopis (FAs 2 and 3), whereas in La Purísima it is mostly represented by late diagenetic dolostones (burial dolomitization) (Machel, 2004) (Fig. 12). The dolomitization observed presents planar fabrics showing planar intercrystalline boundaries, with a mosaic of dolosparite showing dirty crystal cores and clean syntaxial cement regrowth, retaining the pre-dolomitization fabric where the process is partial (Figs. 12A–B). Where the dolomitization is total and the destructive dolomite factory has replaced the original sediments, there is a development of secondary intercrystalline porosity (Fig. 12C). Collectively, these planar fabrics indicate a relatively low temperature of dolomitization  $T \leq 60$  °C (Sibley & Gregg, 1987).

##### Superbundle V – SB V

This package is prograding to the South, strongly dolomitized at La Purísima, with calcarenites in the upper part (FA 1). At the Llopis and Racó Llobet sections, it is composed of well-stratified rudist

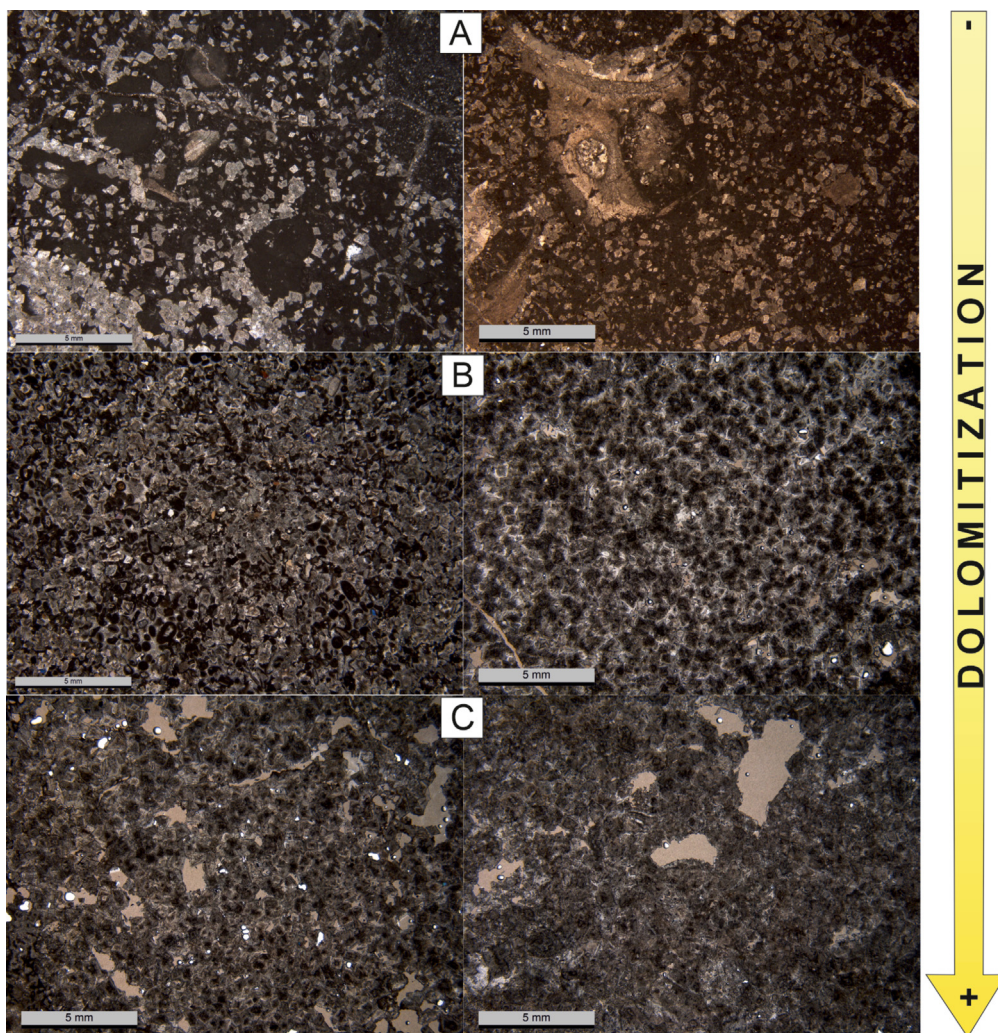


**Fig. 12.** Examples of dolomitization in some of the samples, occurring in La Purísima section. A. Samples LP-59 (left) and LP-70 (right) showing partial dolomitization, as the original sedimentary texture can be recognized. B. Samples LP-64 (left) and LP-63 (right) showing a medium level of dolomitization. The original sedimentary texture is harder to recognize, in the left, it is an ooidal grainstone texture, in the right, only the micritic matrix is distinguished between the dolomite crystals. C. Samples LP-65 (left) and LP-66 (right). In this case, the original depositional texture is completely eradicated, and secondary porosity has been originated.

limestones (FA 3), which alternate with calcarenites at Llopis (FA 2). The rudist facies are very well exposed at Raco Llobet, where this superbundle reaches 30 m thick (Fig. 11E).

#### Superbundle VI – SB VI

This package is 30 m thick at La Purísima, 20 m at Llopis, and 23 m at Raco Llobet. A notable lateral facies change can be observed between them, from the Raco Llobet packstones, rich in rudists and dasycladacean algae, characteristic of inner platform environments (FA 3), to calcarenites with hummocky cross-stratification and marlstones at La Purísima (FA 1) (Fig. 11D).

#### Superbundle VII – SB VII

This set represents the uppermost part of the Middle Member, shown at La Purísima, Llopis, and Agres. It is composed of distal external platform facies (FA 1) at La Purísima (nodular and micritic limestone with biserial benthic foraminifera). At the Raco Llobet section, this superbundle is poorly exposed, and it is dolomitized, so it has not been logged in detail.

#### Superbundle VIII – SB VIII

The Agres Bed is the Upper Member of the Llopis Formation, it crops out at the Agres section and is 8 m thick (Fig. 13). The Agres Bed has a more siliclastic character than the underlying Middle Member of the Llopis Formation (Fig. 14A). It contains some marly and sandy levels between 40 and 80 cm thick and with 5–50 % of

quartz content. Caprinid rudists (*Offneria* sp.) have been distinguished in the uppermost level of this member (Skelton et al., 2019) (Fig. 14B–C), with a marked planar surface atop of it, displaying 4–5 cm diameter sub-spherical borings, and it is colonized by ostreids (Fig. 14D).

#### 4.4. Carbon isotopes

The cross-plots of  $\delta^{13}\text{C}$  vs  $\delta^{18}\text{O}$  (Fig. 15) of Raco Llobet and La Purísima show a low degree of correlation, indicating no intense post-depositional diagenetic alteration or influence of ground-water or meteoric water on the isotopic signature (Jarvis et al., 2011). The Raco Llobet profile describes, from base to top, a generalized positive trend from +1 ‰ to +3 ‰, this type of behaviour before the onset of the OAE 1a has been observed in other carbonate platform records during the early Aptian as the Santa Maria (Abruzzi Region) and Monte Faito (Campania Region) sections from the Central Tethys archives (Amodio & Weissert, 2017).

To connect the C-isotope data of this study with previously published data of the same study area (Castro et al., 2014), the C-isotope profile from Skelton et al. (2019) is presented (Fig. 15), completing the top of the isotopic profile presented in this study.

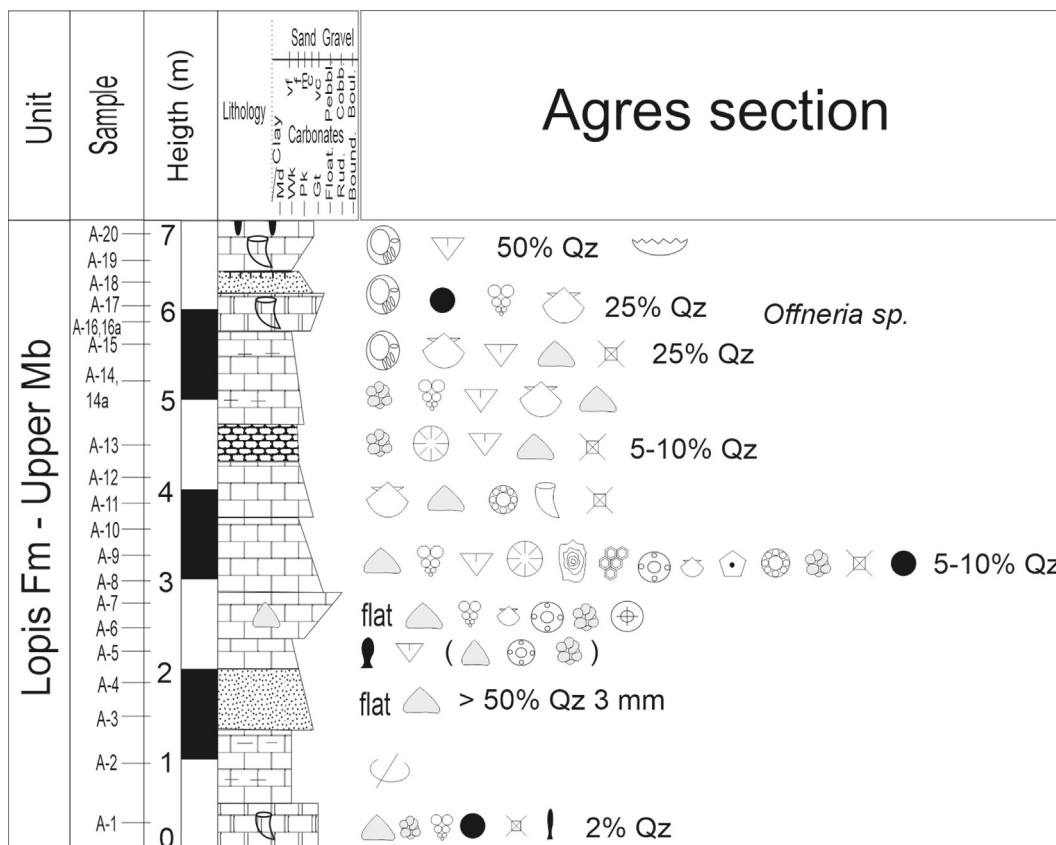


Fig. 13. Detail of the Agres Section showing the Agres Bed, which corresponds to the superbundle VIII of this study.

The correlation uses the top of the Racó Llobet section, as the top of SB VI, which ties-up with the base of SB VII, present in La Purísima, and the top of SB VII, which is overlain by the SB VIII (Agres Bed) in Agres (Fig. 15). The C-isotopes results are described in detail below (see Supplement for detailed carbonate textures).

#### 4.4.1. Racó Llobet

The carbon-isotope record of the Racó Llobet section (Fig. 15) shows pronounced variability along the stratigraphic succession, with values ranging from +0.04 ‰ to +4.08 ‰. The Racó Llobet profile starts with values around +1 ‰ from the base up to 15 m, these are grainstones and facies with corals (FA 2), then, from 15 to 30 m, values are a little higher, around +2 ‰. The variability in this interval is from +3.53 ‰ to +0.42 ‰, because at 20 m two values around +0.5 ‰ in wackestone facies (facies 1) create a transient negative trend of -3.11 ‰. The values then go from +3.12 ‰ to almost 0 (+0.04 ‰ - minimum value of the profile), and then towards +3.34 ‰ (around 50 m), in a negative-positive trend, occurring in Pk and Wk facies (FA 3). Above the former interval, from 50 to 75 m, the three-point moving average profile is steady around +2 ‰, even with sharp peaks in the profile around 55 m (+4.08 ‰ - maximum value of the profile, to 0.41 ‰), with a mix of Pk and Ft facies (FA 3) in the lower part and Gt texture in the upper part (Facies 2). From 75 to 105 m the values seem higher, around +3 ‰, where packstone microfacies (FA 3) dominate within the first 25 m (75–100 m) of this interval, while the upper 5 m (100–105 m) are dominated by wackestones (Facies 5). The uppermost part of section (105 m to top) shows values around +2 ‰, with a high-frequency variability of 2 ‰ amplitude (between +1 ‰ and +3 ‰), presenting a mix of Mt, Wk, Pk textures, and dolostones in the uppermost part.

#### 4.4.2. La Purísima

The carbon isotopic signal at the lower part of La Purísima section (Fig. 15) ranges from +0.43 ‰ to +3.13 ‰. In the lowermost part of the section, the profile marks a negative (+1.98 ‰ to +0.43 ‰) followed by a positive (+0.43 ‰ to +2.83 ‰) trend, sampled in packstone limestones and calcarenites (FA 2). From 125 to 145 m the dolostone interval was not sampled (dolomitization). The uppermost part of the profile (from 150 m to the top) ends with a negative excursion from +3.13 ‰ (maximum value of the profile) to +1.93 ‰, in samples of calcarenites and limestones with corals.

### 5. Discussion

#### 5.1. Facies model

The facies model for the Mariola platform (Fig. 16) corresponds to a biotically-controlled tropical factory (T-factory) (Schlager, 2003, 2005), with a broad flat top characterized by tabular bedding, building out over inclined slope beds (Fig. 11). The tabular to domal, or phaceloid branching colonial corals in FA 2 (Skelton et al., 2019) most likely lived as discrete sediment-dwelling forms, lacking framework construction. Hence the flat-lying platform-top beds passed into the clinofolds of the slope deposits without an intervening salient rim (Fig. 11C; cf., Berra et al., 2016; Shahzad et al., 2019). Nevertheless, the shallow banks of FA 2 on the outer part of the platform top coincided with the transition to the upper slope, where they would have provided frictional attenuation of incoming currents flowing onto the inner platform top (FA 3). The general morphology of the platform reflects the typical greenhouse pattern of growth and demise (Schlager & Philip, 1990;

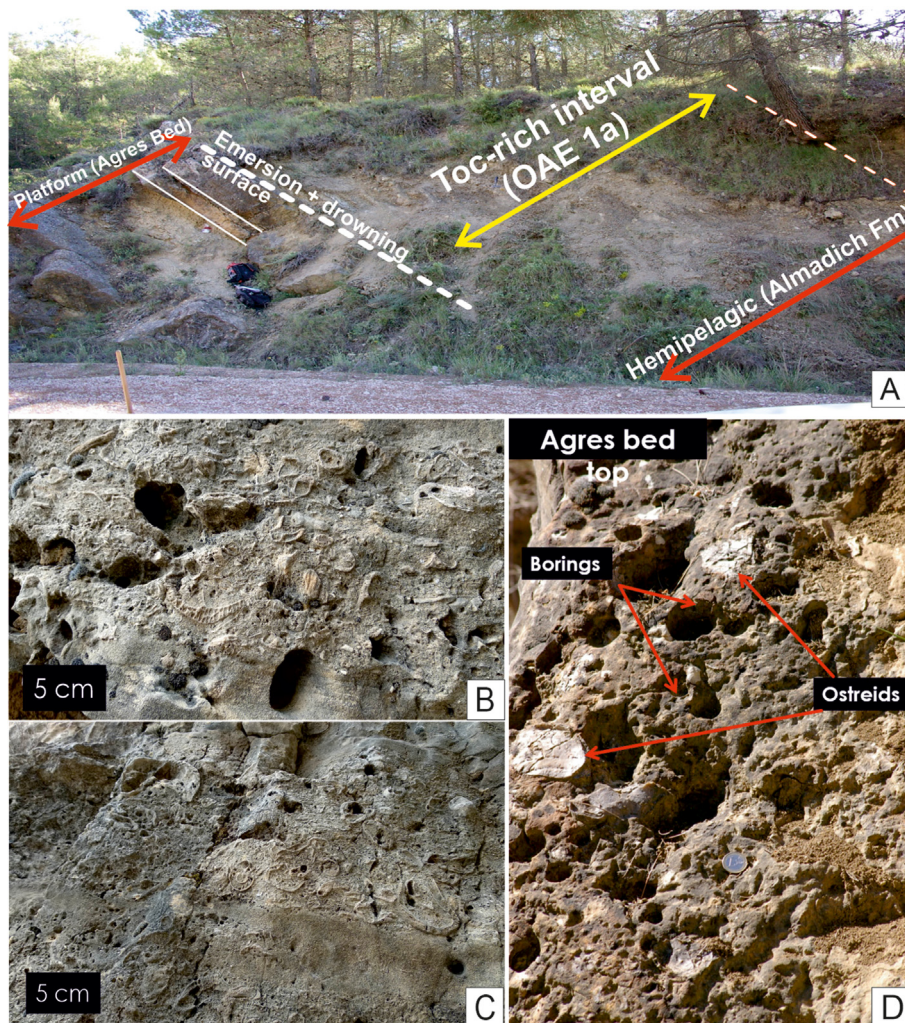


**Fig. 14.** A. Outcrop photography at Agres section showing the top of the Agres Bed and the base of Almadich Fm. B–C. Detail of rudist-rich (*Offneria* sp.) level from the uppermost part of the Agres Bed. D. Top horizon of Agres Bed.

Föllmi et al., 1994; Skelton & Gili, 2012). This type of platform is typically subject to small amplitude eustatic oscillations, associated with extensive lateral redistribution of carbonate sediments, both on and off the platform.

The accumulation of planar/discoidal orbitolinids has been considered related to transgressive trends, which occurred at the end of an important episode of terrigenous input (Vilas et al., 1995). Orbitolinids mostly lived in clear oligotrophic waters (Hallock, 1985), although discoidal orbitolines were better adapted to increased water cloudiness (Hottinger, 1982), and could tolerate siliciclastic influx and mesotrophic conditions (Embry et al., 2010; Pittet et al., 2002). Terrigenous runoff could have increased nutrient supply favouring fast-growing organisms with asexual reproduction, providing a possible scenario for proliferation of larger benthic foraminifera such as planar or discoidal orbitolines (Birkeland, 1988). Facies 1, 2, and 3 collectively represent the platform margin, and facies 2 and 3 represent the transition system that separated the more dynamic open ocean waters from the quieter, low-energy, and shallow-water environments of the inner platform (Reijmer, 2021). In addition, higher sediment production occurred when the top of the platform was flooded (Reijmer et al., 1988; Schlager et al., 1994). The abundance of *Chondrodonta* has been documented in other shallow carbonate platforms from the Western Tethys Realm (Császár et al., 1994; Malchus et al., 1995;

Immenhauser et al., 2004; Gili et al., 2016; Graziano & Raspini, 2018), and its proliferation has been considered as a proxy of environmental instability at the onset of the OAE 1a (Del Viscio et al., 2021).

The facies model described above applies to the Middle Member of the Llopis Fm, whereas the Upper Member corresponds to the sedimentary model of a mixed siliciclastic-carbonate platform with redeposited rudists and other shallow carbonate materials, alternating with sands deposited in open marine conditions. Carbonates were deposited during intervals of low energy, whereas sandstones represent pulses of higher energy with terrigenous inputs and shoal migration.

Collectively, this study depicts a rimless tabular morphology for this platform (Fig. 16), and it constitutes another model example of a flat-topped platform (after Schlager, 2005). This model is consistent with the argument that modern, atoll-type reefs formed in the present icehouse world are not suitable models for greenhouse platforms (Purdy & Winterer, 2001; Skelton & Gili, 2012; Bover-Arnal et al., 2022).

## 5.2. Sedimentary evolution

The Middle and Upper members of the Llopis Fm at Mariola describe two cycles that correspond to two 3rd order sequences

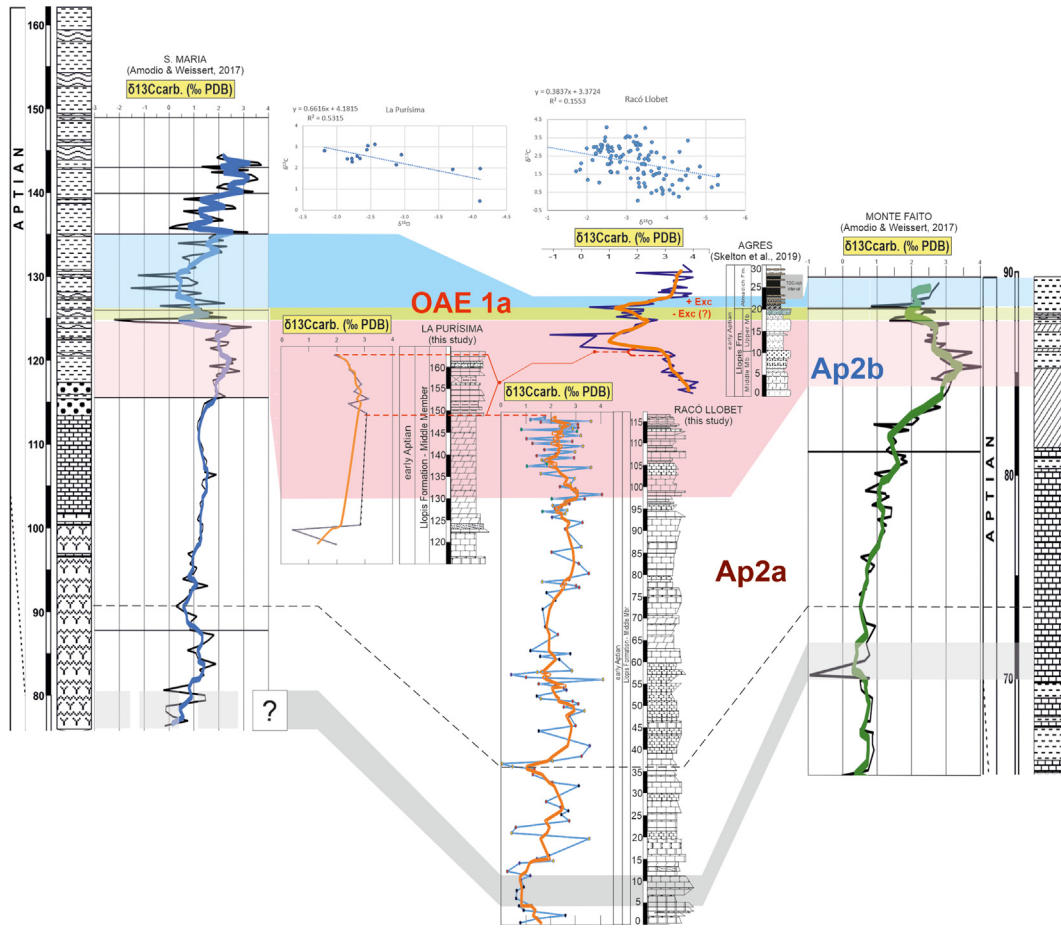


**Fig. 15.** Correlation of C-13 profiles from La Purísima, Racó Llobet (from this study), Agres (modified after Skelton et al., 2019), S. Maria and Monte Faito (modified after Amodio & Weissert, 2017) sections. Orange, blue and green coloured lines indicate the three-point moving average. Cross-plots of  $\delta^{13}\text{C}$  vs  $\delta^{18}\text{O}$  from La Purísima and Racó Llobet are shown on the lower upper middle part. The correspondence with the C-isotope segments (Ap2a and Ap2b) from Castro et al. (2021) is indicated.

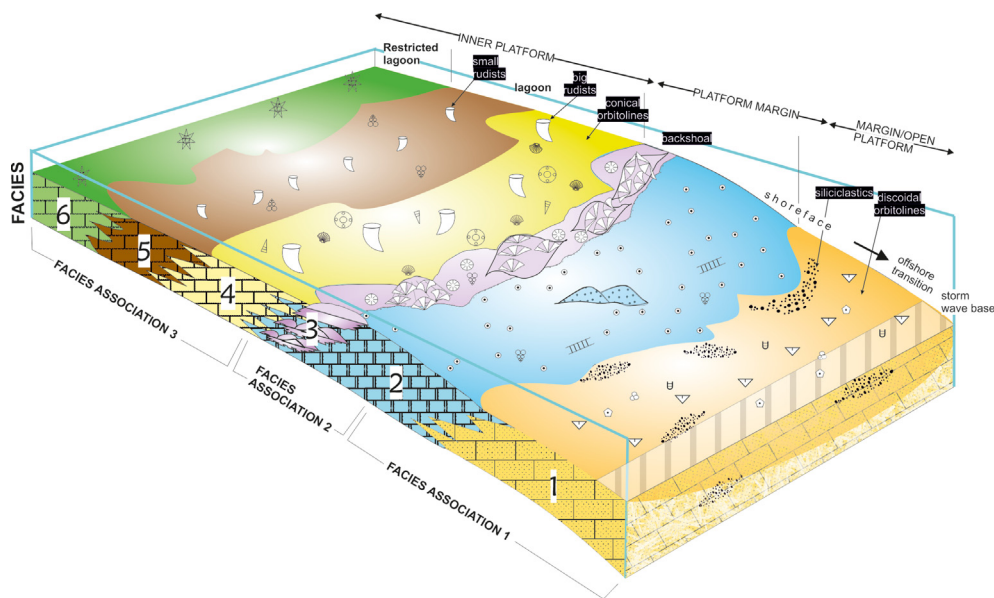


**Fig. 16.** Facies model for the Middle Mb. of the Llopió Fm. Distribution of the facies in a schematic transect through the Mariola platform. The platform model is a flat-topped platform bordered by scattered coral patches formed within the shoal complex, where the break between inner and outer environments is not sharp but gentle. Facies 1: orange; facies 2: blue; facies 3: pink; facies 4: yellow; facies 5: brown; facies 6: green. Facies 7 described in the text belongs to another context of the platform.

(Catuneanu et al., 2009), with a total range of duration for both together of 0.8–1.0 Ma (Hardenbol et al., 1998). The first regressive part of the system involves the installation of an Urgonian platform (superbundle SB I), followed by aggradation and progradation of the internal environments over the open platform (superbundle SB II), in a southwards direction (Fig. 17). Limestones from superbundle I that basically present an aggradational stacking pattern, are overlain by the regressive limestones of superbundle SB II, showing a progradation pulse of more than 1 km southwards; this progradation trend is maintained in the highstand part of superbundle SB II (Fig. 17). Superbundles SB III and IV record a northward migration of the facies belt, defining a transgressive phase. Superbundles V and VI record the second major phase of progradation of the Urgonian shallow carbonate platform. The general trend is a gradual upward retrogradation of the facies belt, as there is retrogradation between superbundles V and VI. At the top of the succession, the Upper Member (Agres Bed) represents the terrigenous input that presaged the demise of the platform, eventually drowned by the hemipelagic deposits of the Almadich Fm.

### 5.3. Cyclostratigraphy – time span estimation

The Llopis platform presents a marked cyclicity that may have an autogenic, allogenic, or mixed origin. In this section, we discuss the possible origin of this cyclicity and the factors that may have affected it. Milankovitch forcing sea-level change due to Earth's orbital variation mechanisms is one of the factors that determine the available accommodation space, via celestial-driven changes in solar radiation (Ruddiman, 2014). Such sea-level changes are arguably the main cause, along with the autogenic shallowing-upwards cyclicity of these carbonates in a subsiding platform (e.g., Reijmer, 2021). The age of the Middle and Upper members of the Llopis Formation is considered to comprise the earliest Aptian (from the base of *M. sarasini* ammonite Zone, equivalent to upper part of the *G. blowi* planktonic foraminifera biozone), to middle Bedoulian (middle early Aptian), including *D. ogranlensis* and the lowermost part of *D. forbesi* ammonite biozone (equivalent to the top of *G. blowi* planktonic foraminifera biozone). This would entail a duration of about 0.8–1 Ma, following the time scale by Gradstein et al. (2020) (Fig. 6), notwithstanding the uncertainty in the time model available for the early Aptian and specifically the base of the Aptian (e.g., Frau et al., 2017; Olierook et al., 2019; Martínez et al., 2020). This duration could involve two 405-kyr long eccentricity metronome cycles and, consequently, the short component of eccentricity periodicity (100-kyr) would coincide with the number (8) of superbundles. Considering the smaller-scale cycles, a total maximum of 33 bundles builds up the 8 superbundles, 26 bundles

from Racó Llobet for SB I to SB VI, plus 7 bundles from Agres (4 bundles from SB VII, and 3 bundles from SB VIII). Considering shorter periodicities as obliquity (40-kyr) and precession (20-kyr), with constant sedimentation, the 0.8–1 My recorded by these materials would include about 20 obliquity cycles and 40 precession cycles. The total maximum stratigraphic cycles found (33), might indicate that cyclicity at this order may be related to an orbital forcing response due to precession (Goldhammer et al., 1991; Wilkinson et al., 1997; Van Wagoner et al., 1998), instead of obliquity, as obliquity is expected not to have substantial influence in variation of insolation received at tropical realms (as Mariola was at a paleolatitude of about 20°N in the Aptian) (Ruddiman, 2014). It should also be mentioned that, in this rifting context, other controlling factors such as subsidence, tectonic, or sediment supply could be responsible for the cyclicity. Furthermore, as 33 bundles have been distinguished, the lack of 7 bundles to reach the ideal 40 cycles, may be because the succession is not continuous, presenting some exposure surfaces. On the other hand, 7 minima of short-eccentricity (100-kyr) could be producing a disguise in cycle detection (Hilgen et al., 2020). Thereupon, elemental cycles that make up the bundles would correspond to auto-cyclic processes within the sedimentary basin, controlled by the interplay between carbonate production and subsidence (e.g., Pratt & James, 1986; Cloyd et al., 1990; Satterley, 1996; Schlager, 2005; Tresch & Strasser, 2011).

#### 5.3.1. Cyclicity discussion

The cyclicity of the platform can be interpreted following methodology and criteria from works by Ajdanlijsky et al. (2020), Bádenas et al. (2005, 2010), Pasquier & Strasser (1997) and Strasser et al. (1999). In the lowermost part of the sections (superbundles I and II), FA 3 developed in a regressive context, describing a fining-upwards association favoring thinner strata in La Purísima (Fig. 18). The lack of detected cycles (bundles – Fig. 18) in La Purísima may be due to dolomitization induced by a fracture; it is likely that the presence of a normal fault between La Purísima and Llopis increased the subsidence of La Purísima but also favoured the introduction of brines that caused dolomitization. In the upper part of the platform, the boundary between superbundles VI and VII is very difficult to establish due to differential subsidence between La Purísima and Llopis (4 bundles) and Racó Llobet (7 bundles), and it has been established following the reactivation surface observed at the top of bundle 7 in Racó Llobet (Fig. 18) along the whole Sierra. In the uppermost part of the sections, at superbundle VII, only 3, 2, and 4 bundles have been recognized in La Purísima, Llopis and Agres respectively (Fig. 18). In this upper part of the transgressive context FA 2 caused the aggradation to predominate over other processes, which is likely responsible for the differential cyclicity.

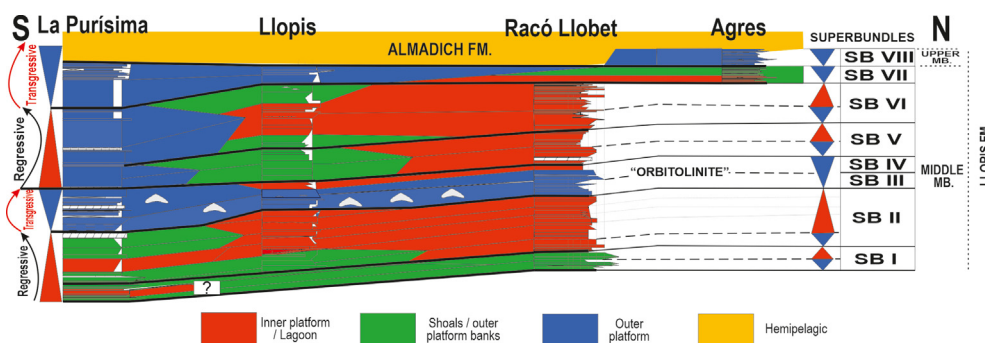
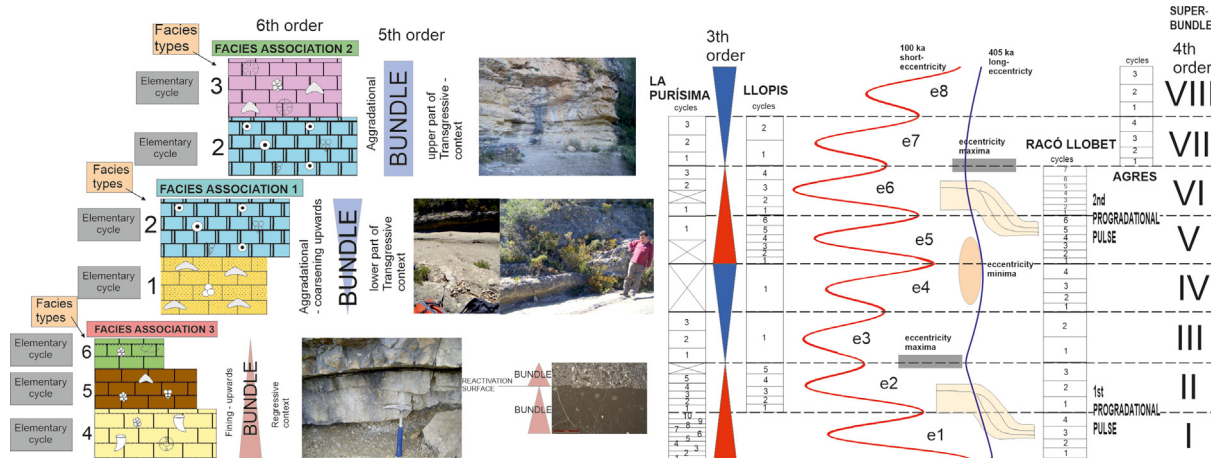


Fig. 17. Sedimentary model for the Middle and Upper Mbs. of the Llopis Fm in Sierra Mariola during early Aptian. The diagram represents a cross-section describing the sedimentary deposition for the 8 superbundles (SB I to SB VIII) in terms of changing sea level (Regression-Transgression) across the 4 studied sections (from S to N and from distal to proximal, respectively; La Purísima, Llopis, Racó Llobet and Agres). The orbitolinid-rich episode is indicated as “orbitolinite” in superbundles SB III and IV.



**Fig. 18.** Left: elementary cycles in terms of facies associations with sequence interpretation. Right: cyclostratigraphic and sequence chart of the studied sections in the Sierra Mariola, part of the Middle and Upper Members of the Llopis Fm. The different cycles (bundles) found are attributable to differential subsidence, lateral facies changes and local factors (see text for explanation). Some intervals are intensely recrystallized and thus multiple bundles are amalgamated in environmentally homogeneous intervals.

Considering each superbundle as representing a 100-ka periodicity of short eccentricity, we interpret that the two 405-ka long eccentricity maxima would correspond to the transgressive regimes (Fig. 18); the first long eccentricity maximum would be associated with the onset of superbundle III, and the second long eccentricity maximum would be related with the onset of superbundle VII, both linked with higher sea levels, promoting transgression and creation of accommodation space for carbonate deposition. Another cyclostratigraphic study from the western Tethys, at Mt. Raggeto section (Campania Apennines), describes 2 superbundles (Fig. 6 from Wissler et al., 2004) from the Barremian to the base of the Selli Level Equivalent (base of the OAE 1a). Those authors assumed that superbundles represented long eccentricity periodicity of 400 ka, so, in terms of time calibration, the duration of this interval would be similar, with 0.8 Ma (two 0.4 Ma long eccentricity cycles) from the Barremian-Aptian boundary to the base of the Selli Event. However, there is a difference in the sedimentary rate between sections, as this interval presents 20 m of thickness at Mt. Raggeto while in Mariola the thickness is 175 m. Another study from Urganian platforms in inner mixed carbonate-siliciclastic successions from Zonguldak (NW Turkey) (Yilmaz & Altiner, 2007) describes 13 cycles from the Barremian-Aptian boundary to the Ap 3 sequence chronostratigraphy stage from Graciansky et al. (1999), that roughly corresponds to the OAE 1a. These authors assume, for the Çengilledere section, a duration of 1 Ma for this interval (Fig. 13 from Yilmaz & Altiner, 2007), interpreting these cycles as 4th-order cycles, and assuming a duration for each one of these cycles of 115–200 ka (short eccentricity). In this case, with a thickness of 50 m, the sedimentary rate from the Çengilledere section is lower than Mariola, but the interpretation in terms of Milankovitch cyclicity agrees more with the approach of this study.

5.4. Control factors over sedimentation and cyclicity

The first superbundle (SB I) is composed of inner and margin platform facies at La Purísima, margin facies at Llopis, and inner platform facies at Racó Llobet. The grainstones at Llopis showing very well-sorted ooids (Facies 2) indicate agitated, shallow waters. This superbundle shows a marked cyclicity, especially in bundles BR1 to BR4 at Racó Llobet (Fig. 4), which represents a highstand phase with thinning- and shallowing-upwards sequences (e.g. Frago et al., 2021). Each bundle top is a planar surface, associated with bioturbation, borings, reddish colours, and irregular morphology, indicating a sedimentary interruption, probably

linked to a drop in relative sea level. At the southern part of the outcrops, in La Purísima section, SB I present ten bundles (BLP1 to BLP10) (Fig. 4). Higher quartz content and marly levels, overall, in the lower part (bundles BLP1 to 6) could reflect a rising sea-level phase (Fig. 17). These carbonates deposited under high turbidity waters, rich in nutrients, and therefore limited carbonate production, favoured the thriving of ecologically opportunistic organisms, such as planar orbitolines (Funk et al., 1993; Vilas et al., 1995; Bernaus et al., 2000). Bundles from the upper part (BLP7 to 10) show inner platform facies (Fig. 4) and are related to a more stable phase of sea level without significant siliciclastic input. The upper part of the SB I from La Purísima is difficult to correlate with the Llopis section (Fig. 4), indicating a possible hiatus or erosional gap in the middle part of the platform at Llopis and Racó Llobet, a common feature in shallow platforms (Strasser, 2015, 2018), implying the regressive character of the basin at that time. The absence of these upper bundles at Llopis and Racó Llobet sections may also be linked with postdepositional erosion due to synsedimentary tectonics (uplift) related to the top of an unconformity.

The second superbundle (SB II) has a similar development to the first one: the three bundles BR5 to BR7 of the internal platform at Racó Llobet laterally correlate to five bundles BLP11 to BLP15 of a more distal character at La Purísima (Fig. 4). Between the Racó Llobet and La Purísima section, the Llopis section records a change from open platform environments (BL1 to BL3) to inner platform conditions (BL4 and BL5), recorded by lateral facies change across clinofolds (Fig. 11C). As the regression progressed, the decreasing turbidity and a better connection to more open marine waters drove a change to optimum environmental conditions for carbonate production, under a warm climate, stimulating the carbonate factory and producing higher sedimentation rates (SB II doubles the thickness of SB I at Racó Llobet, while at La Purísima SB I and SB II are 40 m thick) (Fig. 4); however, an increase in subsidence rates may be also taken into account to explain such increase in thickness. The lower half of SB II at Racó Llobet is mainly formed by the BR5 cycle, with calcarenitic coral-rich rudstone and grainstone facies. The upper half of SB II at Racó Llobet is composed of one thick cycle (BR6 and BR7), limited to micritic limestones with rudist and miliolid fauna, reflecting a general trend to slightly more restricted environments. This step from corals to rudists is linked to an environmental change, as corals live generally in oligotrophic conditions (except platy corals, Rosen et al., 2000) while rudists tolerate higher nutrient and turbidity conditions (e.g., Gili et al., 1995; Pittet et al., 2002). The vertical facies change noted herein is interpreted as the result of a shallowing-

upward evolution. The increase in the restriction of the waters might be linked to an aggradation in the margin zone (Llopis), that would make difficult the connection between the inner and external parts of the platform. This change is also reflected in the distal sector of La Purísima: in SB II the bundles B<sub>LP</sub>11 to B<sub>LP</sub>13 display open shoal banks platform facies (association of *Derventina*, *Sabaudia* and *Choffatella*, along with planar orbitolinids). With this information, during the lower part of SB II, the limit between inner and external environments is placed between the Llopis and Racó Llobet sections. In the upper part of SB II, the cycles B<sub>LP</sub>14 and B<sub>LP</sub>15, are generally thicker than the lower cycles (Fig. 4), with the dominance of ooid-rich calcarenites, reflecting the progradation of internal facies over the outer platform facies (Fig. 17). In terms of paleoecology, this regressive part formed by SB I and II is dominated by miliolids, extreme K-strategists thriving in oligotrophic environments with some quartz content (Skelton et al., 2003b) or no siliciclastic input (Wilmsen, 2000; Parente et al., 2008).

Superbundles SB III and IV are key to understanding the general evolution of the platform, with a marked transgressive character. SB III is intensely dolomitized at La Purísima, whereas at Llopis bundle B<sub>L</sub>6 shows an open platform association of facies 1 and 2, with *Choffatella decipiens* and *P. maynci* (Castro, 1998). At Racó Llobet, SB III is composed of 2 bundles, B<sub>R</sub>9 and B<sub>R</sub>10, both with abundant brachiopods in the lower part and calcarenite beds at the top. SB III has a transgressive character, with nodular limestones and brachiopods, that represent an increase in bathymetry. These cycles are interpreted as shallowing upwards, with a progressive increase in water energy (nodular limestones to calcarenites). This superbundle represents the beginning of a new T-R depositional sequence for the Middle Member, from progradation in the lower half to retrogradation in the upper half (Fig. 17).

Superbundle SB IV represents a homogeneous sedimentary episode, with the dominance of open platform facies. At Racó Llobet, bundles B<sub>R</sub>11 and B<sub>R</sub>12 present open marine facies association, dominated by orbitolines, and B<sub>R</sub>13 has abundant echinoderms and quartz (Fig. 4). Collectively, these marly lithofacies, plenty of planar orbitolines with crinoids, indicate open marine conditions, with moderate energy, and they are associated to a transgressive episode, resulting in homogeneous sedimentation within the studied area.

At a higher scale, the change in peritidal and shallow subtidal cycles from SB I and II to more distal facies in SB III and SB IV are linked to an increase in the siliciclastic input in the platform, probably coeval to increased subsidence rates, which affected the carbonate production and reduced or removed the shoal banks system at the edge of the platform. Under these conditions, external platform deposits were dominant in the area studied. At La Purísima, cycles B<sub>LP</sub>16, B<sub>LP</sub>17 and B<sub>LP</sub>18 display hummocky cross-stratification and planar orbitolines (FA 1) (Fig. 4). At Llopis, B<sub>L</sub>7 contains grainstone and packstone limestones with *O. buccifer* (Fig. 4). Bundles B<sub>L</sub>4 and B<sub>L</sub>5 show a mixing of globular and conical orbitolines (*Paracoskinolina maynci* with *O. praesimplex* and *buccifer*) (Fig. 4), which might represent the proximal sedimentary expression of the storm deposits from La Purísima. Collectively, this “orbitolinite” facies enriched in siliciclastics, represent an important change in the carbonate production (from oligotrophic to mesotrophic conditions) and could be attributed to the intensified hydrological cycle and continental weathering under warm and more humid conditions (Heimhofer et al., 2008; Tejada et al., 2009; Stein et al., 2012; Bottini et al., 2015; Lechler et al., 2015), probably combined with a relative rising sea level and transgressive conditions (e.g. Vilas et al., 1995). This episode may be linked to a regional climatic event, as other orbitolinid blooms have been recorded from the Northern Tethys (Föllmi et al., 2006) and the North

Atlantic (Millán et al., 2011), related to the environmental changes heralding the OAE 1a (e.g., Najarro et al., 2011a; Amodio and Weissert, 2017; Föllmi, 2012; Martínez-Rodríguez et al., 2021; de Gea et al., 2024).

Within superbundle SB V, only bundle B<sub>LP</sub>19 has been recognized at La Purísima, at the uppermost part, which contains facies 2 and 3 with *Orbitolinopsis praesimplex* and cortoids (Fig. 4). At Llopis, SB V displays facies 1, 2, 4 and 5. In detail, bundle B<sub>L</sub>8 contains a calcarenite association with *Orbitolinopsis cuvillieri*, while B<sub>L</sub>9 contains also orbitolinids, and B<sub>L</sub>10 contains *Orbitolinopsis praesimplex* (Fig. 4). Bundles B<sub>L</sub>11 and B<sub>L</sub>12 present some levels enriched in quartz (Fig. 4), indicating an intermittent clastic input. At Racó Llobet, the lower part of the superbundle contains *O. buccifer*, quartz, and echinoids, whereas the upper part is dominated by micritic facies 4 and 5, with abundant dasycladacean algae and biseriate benthic foraminifera (Fig. 4). On this superbundle, the cyclicity of strata starts to be more marked than below, with thinner beds, probably due to a reduction in the accommodation space, in a regressive context (Fig. 17).

In La Purísima, at the base of superbundle SB VI, bundle B<sub>LP</sub>20 records the presence of sandy orbitolines (Fig. 4). Quartz is also found at Llopis in bundles B<sub>L</sub>14 to B<sub>L</sub>17 (Fig. 4), confirming that the terrigenous input is being produced not only in the lower transgressive part of the superbundle, but also during the upper regressive part (Fig. 17). All the studied sections are dominated by rudist facies (*Toucasia* and *Caprina douvillei* are present), despite the stressed environment as inferred from the presence of terrigenous sediments, contradicting the idea of rudists as fauna that grows only in siliciclastic-free oligotrophic environments (van Buchem et al., 2002; Rameil et al., 2010; García-Penas et al., 2024). Circulation in the platform should have been likely good enough to rapidly dissipate the environmental stress associated with the detrital input, increasing the salinity and allowing planktonic rudist larvae to thrive (Gili & Götz, 2018).

During the deposition of superbundle SB VII, the lagoonal and internal platform environments were progressively replaced by platform-shoals and open platform environments, as facies 1 and 2 with arenaceous orbitolines and intraclasts dominate (Fig. 4). This is interpreted as the result of retrogradation of the platform system (Fig. 17), in which the facies belts retract as a response to a relative sea-level rise, probably related to a combination of climatic and tectonic factors, with the initiation of an extensional tectonic event with activation of listric faults (Vera, 2004; Castro et al., 2008; Granier & Perthuisot, 2009), and a humidity increase in the continent (Aguado et al., 2014; Castro et al., 2019) with the subsequent terrigenous input to the platform, processes that culminated in the next superbundle.

The superbundle SB VIII (Agres Bed) testifies to a definitive change in the Urganian platform. High detrital input and the installation of open marine facies mark the end of favorable environmental conditions for the Urganian platform, resulting in low carbonate productivity. Sandstone levels with fragments of large caprinids (*Offneria* sp.) (Figs. 13, 14) deposited under high energy conditions, indicate a complex evolution with quiet phases of high carbonate production, which alternated with higher energy episodes in which important terrigenous input hampered the carbonate production. These rapid fluctuations are typical of unstable and unpredictable environments characterized by significant changes in trophic resources produced by hyperthermals (Leckie et al., 2002; Posenato et al., 2018; García-Garnica & Pérez-Cruz, 2022). A similar change in carbonate factories documented in the Barremian-Aptian strata from the Arabian plate has been ascribed to siliciclastic influx and changing nutrient levels (van Buchem et al., 2002).

## 5.5. Carbon isotopes

Despite the low correlation in the C and O isotope cross-plots (Fig. 15), the presence of significant variability and sharp peaks in the carbon profiles prevents completely ruling out the absence of diagenetic overprinting. Although intervals with dolostones were avoided, the presence of brines that could have circulated through fractures may have altered the original isotopic signal without a perceptible petrographic variation. Besides, the bioclastic character of some of the samples may have introduced noise into the data due to the difficulty of sampling only in the micrite matrix.

The most reliable part of the dataset is the top of La Purísima section, which describes a decreasing trend from +3 ‰ to +2 ‰, which correlates, with an expanded character, with the negative trend from the uppermost part of the Middle Mb within the Agres section (Fig. 15). Collectively, the C-isotope profile from this study (Middle Mb of the Llopis Fm) corresponds to the defined Ap2 (Castro et al., 2021) segment (C2 segment after Menegatti et al., 1998). Although the overall variability in the data from the Racó Llobet section, with a range of roughly 3.5 ‰ points (Fig. 15), is higher than other C-isotope profiles from a carbonate platform context (for the same Ap2/C2 segment), such as the ODP Site 866 (Jenkyns, 1995), with ca. 2.5 ‰ of variation, other sections from an intra-shelf basin context show sharp peaks in the  $\delta^{13}\text{C}$ , such as the Cau section, with peaks between approx. +1 ‰ to +3.25 ‰ (Castro et al., 2021). Nevertheless, the three-point average data between +2 ‰ and +3 ‰ (Fig. 15) within the C2/Ap2 segment are consistent with other records such as La Bédoule Core (Lorenzen et al., 2013), Peregrina Canyon (Bralower et al., 1999), both from an intra-shelf basin context, and with the Piobbico and Cison cores (Bottini et al., 2015), from a deep pelagic basin context.

The main result from the new C-isotope stratigraphy of the middle member of the Llopis Fm is the confirmation that the Agres Bed coincides with the base of the Ap3 segment, as proposed by Skelton et al. (2019) from the study of the overlying Agres bed and Almadich Fm. Thus, this major sedimentary change is interpreted as the local expression of the onset of the OAE 1a. As a hyperthermal, the facies found in the Agres section are consistent with intensified global greenhouse climatic pattern occurred in response to a major perturbation in the C-cycle (e.g., Menegatti et al., 1998; Jenkyns, 2010; Bottini et al., 2015; Erba et al., 2015; Castro et al., 2021; Martínez-Rodríguez et al., 2021, 2024).

### 5.5.1. Tethys correlation

The sections investigated in this study are correlated with two sections from the Western Tethys: the Santa Maria and the Monte Faito sections (Urgonian carbonate platform, Italy, Amodio & Weissert, 2017). These sections mostly represent the Ap2 (C2 from Menegatti et al., 1998) C-isotope segment. This interpretation is based on the moving average values, not on specific punctual values.

In the lower part of the sections, the Ap2a segment describes a long-term positive trend from values near 0 to +2 ‰ in the sections from the central-southern Apennines, whereas in the sections from Mariola, this trend goes from +1 to +3 ‰ (Fig. 15). A stable interval (from 5 to 10 m) around +1 ‰ at Racó Llobet correlates with a 2-m interval (70–72 m) around +0.5 ‰ at M. Faito, which is roughly correlated with the base of the S. Maria section (Fig. 15). Some meters above, a double negative-positive trend, with the turning point around +1 ‰ at metre 36 of Racó Llobet, correlates with a level around +0.5 ‰ in S. Maria and M. Faito sections (at metres 92 and 73.5, respectively).

In the upper part of the sections, segment Ap2b corresponds to a decreasing trend, from values near +3–3.5 ‰, to approximately +2 ‰ in all the sections (Fig. 15). This excursion

precedes the sharper and more rapid negative excursion which marks the onset of the OAE 1a (see Castro et al., 2021; Martínez-Rodríguez et al., 2021), only recorded in the Sierra Mariola at the Agres section (Skelton et al., 2019).

## 6. Conclusions

The study of four sections of the Llopis Fm distributed in the outcrops of Sierra Mariola allows the recognition of facies and facies associations of open platform, margin, and inner platform environments from the lower Aptian Urgonian carbonate platform formed in the southern Iberian margin. The analysis of facies belts, the stratigraphic architecture, and the sedimentary model points to flat-topped carbonate platform type for the Aptian platform in Sierra Mariola.

Up to eight superbundles (4th order cycles) are described in the study. The time interval of the sedimentation of the studied succession is considered to span ~0.8–1 Ma, interpreted to encompass approximately two long eccentricity orbital cycles, with each superbundle representing ~100-kyr short eccentricity cycles. The two long eccentricity maxima coincide with major transgressive trends within the platform.

The  $\delta^{13}\text{C}$  data from the Middle member of the Llopis Fm confirm that this unit records the Aptian Ap2 C-isotope segment that precedes the OAE 1a. The onset of OAE 1a is coeval with the upper part of the Agres Bed (Upper Mb), which represents the local sedimentary expression of the onset of the OAE 1a, which eventually led to the demise of the Llopis Fm carbonate platform with the deposition of the hemipelagic marls of the overlying Almadich Fm.

Discussion concerning the factors that regulated the formation and subsequent demise of the early Aptian carbonate platform highlights the intricate interplay between regional extensional tectonics (subsidence), climate, and environmental changes leading to different modes of carbonate production controlled by variations in the siliciclastic input, and relative sea-level changes. The Mariola platform witnesses a *Chondrodonta* event and an orbitolinid episode recorded in other parts of the Tethys. The utmost environmental change is intricately linked and coeval with the global OAE 1a, a major perturbation that resulted in the demise of the carbonate platform and the onset of hemipelagic sedimentation.

The findings of this study demonstrate that despite the considerable climatic fluctuations that occurred before the onset of OAE 1a, shallow carbonate platforms persisted in their ability to adapt to changing conditions and evolved, thereby underscoring the remarkable resilience and adaptability of these ecosystems in the face of relatively rapid environmental shifts.

The potential future applications of this research include forward modelling (with a photogrammetric study and a 3D numerical model) for this platform. Another possibility is to do an evenly-spaced sampling (5–10 cm) to analyse properties such as  $\text{CaCO}_3$  content or magnetic susceptibility. This would allow spectral and harmonic analysis of time series, which would refine the cyclicity identified through petrography to align with astronomical calibration.

### CRedit authorship contribution statement

**Rafael Martínez-Rodríguez:** Writing – review & editing, Writing – original draft, Validation, Software, Methodology, Investigation, Formal analysis, Data curation, Conceptualization. **José M. Castro:** Writing – review & editing, Visualization, Validation, Supervision, Resources, Methodology, Investigation, Formal analysis, Conceptualization. **Ginés A. de Gea:** Writing – review & editing, Supervision, Methodology, Investigation. **Luis M. Nieto:** Writing – review & editing, Validation, Supervision. **Pedro A. Ruiz-**

**Ortiz:** Supervision, Project administration, Funding acquisition.  
**Peter W. Skelton:** Writing – review & editing, Conceptualization.

### Declaration of competing interest

The authors declare that they have no known competing financial interests or personal relationships that could have appeared to influence the work reported in this paper.

### Acknowledgments

The authors wish to express special thanks to the Natural Park of Sierra Mariola (Valencian Community) for granting access to the different outcrops. This work was a contribution to the PhD thesis of the first author, within the research group RNM-200 “Basin Analysis and Environmental Geology”. Our acknowledgement to Antonio Piedra Martínez, technician of the laboratory of geology (University of Jaén), for the preparation of thin sections, and to technicians Aitor Antón and Rodolfo Pozuelo from the Stable Isotope Laboratory (IGEO–CSIC–UCM). Funding for this study was provided by project CGL 2014-55274-P of the Spanish Ministry of Science and Technology, project 06.17.02.80.P1 of the University of Jaén and FEDER, and a PhD-student scholarship from the University of Jaén (Spain) given to RMR. We deeply thank the journal reviewers and editors for their helpful comments in improving the manuscript. In memory of Professor Luis Pomar.

### Data availability

The data is provided in the supplementary file.

### References

- Aguado, R., de Gea, G.A., Castro, J.M., O'Dogherty, L., Quijano, M.L., Naafs, B.D.A., Pancost, R.D., 2014. Late Barremian–early Aptian dark facies of the Subbetic (Betic Cordillera, southern Spain): Calcareous nannofossil quantitative analyses, chemostratigraphy and palaeoceanographic reconstructions. *Palaeogeography, Palaeoclimatology, Palaeoecology* 395, 198–221. <https://doi.org/10.1016/j.palaeo.2013.12.031>.
- Ajdanlijsky, G., Strasser, A., Götz, A.E., 2020. Sequence analysis, cyclostratigraphy and palynofacies of early Anisian carbonate ramp deposits, NW Bulgaria. *Annales Societatis Geologorum Poloniae* 90 (4), 347–379. <https://doi.org/10.14241/ASGP.2020.27>, 10.14241/asgp.2020.27.
- Alonso-Chaves, F., Andreo Navarro, B., Azañón Hernández, J., Balanyá Roure, J., Booth Rea, G., Crespo Blanc, A., Delgado, F., Diaz De Federico, A., Estévez, A., Galindo Zaldívar, J., García Casco, A., García Dueñas, V., Garrido, C., Gervilla Linares, F., González Lodeiro, F., Jabaloy Sánchez, J., Martín Algarra, A., Marfín Martín, M., O'dogherty Luy, L., Vera Torres, J., 2004. Zonas Internas Béticas. In: *Geología de España*, pp. 395–396.
- Amodio, S., Weissert, H., 2017. Palaeoenvironment and palaeoecology before and at the onset of Oceanic Anoxic Event (OAE)1a: Reconstructions from Central Tethyan archives. *Palaeogeography, Palaeoclimatology, Palaeoecology* 479, 71–89. <https://doi.org/10.1016/j.palaeo.2017.04.018>.
- Armella, C., Cabaleri, N., Leanza, H., 2008. Facies de patch reefs en la Formación Picún Leufú (límite Jurásico/Cretácico) en la región de Zapala, Cuenca Neuquina. *Revista del Museo Argentino de Ciencias Naturales Nueva Serie* 10 (1), 63–70. <http://revista.macn.gov.ar/ojs/index.php/RevMus/article/view/293>.
- Arnaud-Vanneau, A., 2005. Environmental controls on tropical carbonate platform. In: Adatte, T., Arnaud-Vanneau, A., Arnaud, H., Blanc-Aletru, S., Bodin, S., Carrioch-Schaffhauser, E., Föllmi, K.B., Godet, A., Raddadi, M.C., Vermeulen, J. (Eds.), *The Hauterivian-Lower Aptian Sequence Stratigraphy from Jura Platform to Vocontian Basin: A Multidisciplinary Approach*, vol. 7, pp. 29–78. *Géol. Alpine, Sér. Spéc. “Colloques Excursions*.
- Azéma, J., 1971. Le Jurassique dans la partie orientale des zones externes des Cordillères Bétiques le prébetique de Cieza à Alicante. *Cuadernos de Geología Iberica* 2, 111–124.
- Bádenas, B., Aurell, M., Bosence, D., 2010. Continuity and facies heterogeneities of shallow carbonate ramp cycles (Sinemurian, Lower Jurassic, North-east Spain). *Sedimentology* 57 (4), 1021–1048. <https://doi.org/10.1111/j.1365-3091.2009.01129.x>.
- Bádenas, B., Aurell, M., Gröcke, D.R., 2005. Facies analysis and correlation of high-order sequences in middle–outer ramp successions: variations in exported carbonate on basin-wide  $\delta^{13}\text{C}_{\text{carb}}$  (Kimmeridgian, NE Spain). *Sedimentology* 52 (6), 1253–1275. <https://doi.org/10.1111/j.1365-3091.2005.00740.x>.
- Bathurst, R.G.C., 1975. Carbonate sediments and their diagenesis. In: *12Dev. Sedimentol. Elsevier*.
- Beresi, M.S., Cabaleri, N.G., Löser, H., Armella, C., 2017. Coral patch reef system and associated facies from southwestern Gondwana: paleoenvironmental evolution of the Oxfordian shallow-marine carbonate platform at Portada Covunco, Neuquén Basin, Argentina. *Facies* 63 (1), 1–22. <https://doi.org/10.1007/S10347-016-0486-4/FIGURES/9>.
- Bernaus, J.M., Caus, E., Arnaud-Vanneau, A., 2000. Aplicación de los análisis micropaleontológicos cuantitativos en estratigrafía secuencial: El Cretácico inferior de la cuenca de Organyà (Pirineos, España). *Rev. Soc. Geol. Esp* 13, 55–63.
- Berra, F., Lanfranchi, A., Smart, P.L., Whitaker, F.F., Ronchi, P., 2016. Forward modelling of carbonate platforms: sedimentological and diagenetic constraints from an application to a flat-topped greenhouse platform (Triassic, Southern Alps, Italy). *Marine and Petroleum Geology* 78, 636–655.
- Birkeland, C., 1988. Second-order ecological effects of nutrient input into coral communities. *Galaxea* 7 (2), 91–100.
- Bond, G.C., Kominz, M.A., 1984. Construction of tectonic subsidence curves for the early Paleozoic miogeocline, southern Canadian Rocky Mountains: Implications for subsidence mechanisms, age of breakup, and crustal thinning. *GSA Bulletin* 95 (2), 155–173. [https://doi.org/10.1130/0016-7606\(1984\)95<155:COTSCF>2.0.CO;2](https://doi.org/10.1130/0016-7606(1984)95<155:COTSCF>2.0.CO;2).
- Bonvallet, L., Arnaud-Vanneau, A., Arnaud, H., Adatte, T., Spangenberg, J.E., Stein, M., Godet, A., Föllmi, K.B., 2019. Evolution of the Urganian shallow-water carbonate platform on the Helvetic shelf during the late Early Cretaceous. *Sedimentary Geology* 387, 18–56. <https://doi.org/10.1016/j.sedgeo.2019.04.005>.
- Bosence, D.W.J., Wood, J.L., Rose, E.P.F., Qing, H., 1999. Low- and high-frequency sea-level changes control peritidal carbonate cycles, facies and dolomitization in the Rock of Gibraltar (Early Jurassic, Iberian Peninsula). *Journal of the Geological Society* 157 (1), 61–74. <https://doi.org/10.1144/JGS.157.1.61>.
- Bottini, C., Erba, E., Tiraboschi, D., Jenkyns, H.C., Schouten, S., Sinnighe Damsté, J.S., 2015. Climate variability and ocean fertility during the Aptian Stage. *Climate of the Past* 11 (3), 383–402. <https://doi.org/10.5194/CP-11-383-2015>.
- Bover-Arnal, T., Salas, R., Guimera, J., Moreno-Bedmar, J.A., 2022. Eustasy in the Aptian world: A vision from the eastern margin of the Iberian Plate. *Global and Planetary Change* 214, 103849. <https://doi.org/10.1016/j.gloplacha.2022.103849>.
- Bralower, T., CoBabe, E., Clement, B., Sliter, W., Osburn, C., Longoria, J., 1999. The record of global change in mid-Cretaceous (Barremian-Albian) sections from the Sierra Madre, Northeastern Mexico. *Journal of Foraminiferal Research* 29.
- Busnardo, R., Champetier, Y., Fourcade, E., Moullade, M., 1968. Étude stratigraphique des faciès a orbitolinides et a rudistes de la Sierra Mariola (province d'Alicante, Espagne). *Geobios* 1 (1), 165–185. [https://doi.org/10.1016/S0016-6995\(68\)80006-3](https://doi.org/10.1016/S0016-6995(68)80006-3).
- Castro, J.M., 1998. Las plataformas del Valanginiense superior-Albiense superior en el Prebético de Alicante. *Universidad de Granada*.
- Castro, J.M., Company, M., De Gea, G.A., Aguado, R., 2001. Biostratigraphy of the Aptian–Middle Cenomanian platform to basin domain in the Prebetic Zone of Alicante, SE Spain: calibration between shallow water benthonic and pelagic scales. *Cretaceous Research* 22 (2), 145–156. <https://doi.org/10.1006/CRES.2000.0249>.
- Castro, J.M., de Gea, G.A., Quijano, M.L., Aguado, R., Froehner, S., Naafs, B.D.A., Pancost, R.D., 2019. Complex and protracted environmental and ecological perturbations during OAE 1a - Evidence from an expanded pelagic section from south Spain (Western Tethys). *Global and Planetary Change* 183, 103030. <https://doi.org/10.1016/j.gloplacha.2019.103030>.
- Castro, J.M., de Gea, G.A., Ruiz-Ortiz, P.A., Nieto, L.M., 2008. Development of carbonate platforms on an extensional (rifted) margin: the Valanginian–Albian record of the Prebetic of Alicante (SE Spain). *Cretaceous Research* 29 (5–6), 848–860. <https://doi.org/10.1016/j.cretres.2008.05.012>.
- Castro, J.M., Jiménez de Cisneros Vencelá, C., de Gea Guillén, G.A., Ruiz Ortiz, P.A., Quijano, M.L., Caballero Mesa, E., Pancost, R.D., 2014. La Formación Almadich en la Sierra de Mariola: caracterización litológica, bioestratigráfica, geoquímica y mineralógica (Aptiense Inferior, Cordillera Bética, Alicante). *Revista de la Sociedad Geológica de Espana* 27, 127–136.
- Castro, J.M., Ruiz-Ortiz, P.A., de Gea, G.A., Aguado, R., Jarvis, I., Weissert, H., Molina, J.M., Nieto, L.M., Pancost, R.D., Quijano, M.L., Reolid, M., Skelton, P.W., López-Rodríguez, C., Martínez-Rodríguez, R., 2021. High-Resolution C-Isotope, TOC and Biostratigraphic Records of OAE 1a (Aptian) From an Expanded Hemipelagic Cored Succession, Western Tethys: A New Stratigraphic Reference for Global Correlation and Paleoenvironmental Reconstruction. *Paleoceanography and Paleoclimatology* 36 (3), e2020PA004004. <https://doi.org/10.1029/2020PA004004>.
- Catuneanu, O., Abreu, V., Bhattacharya, J.P., Blum, M.D., Dalrymple, R.W., Eriksson, P.G., Fielding, C.R., Fisher, W.L., Galloway, W.E., Gibling, M.R., Giles, K.A., Holbrook, J.M., Jordan, R., Kendall, C.G.S.C., Macurda, B., Martinsen, O.J., Miall, A.D., Neal, J.E., Nummedal, D., Winker, C., 2009. Towards the standardization of sequence stratigraphy. *Earth-Science Reviews* 92 (1–2), 1–33. <https://doi.org/10.1016/j.earscirev.2008.10.003>.
- Cloyd, K.C., Demicco, R.V., Spencer, R.J., 1990. Tidal channel, levee, and crevasse-splay deposits from a Cambrian tidal channel system; a new mechanism to produce shallowing-upward sequences. *Journal of Sedimentary Research* 60 (1), 73–83. <https://doi.org/10.1306/212F9115-2B24-11D7-8648000102C1865D>.

- Company, M., Garúa-Hernández, M., López-Garrido, A.C., Vera, Y.A., Wilke, I.L., 1982. Interpretación genética y paleogeográfica de las Turbiditas y materiales redepósitos del Senonense superior en la Sierra de Aixorta (Prebético interno, provincia de Cuadernos de Geología Iberica 8, 449–463. <https://digital.csic.es/handle/10261/5911>.
- Császár, G., Mhel, D., Oberhauser, R., Lobitzer, H., 1994. A comparative study of the Urganian Facies in Vorarlberg (Austria), in Allgäu (Germany) and in the Villány Mountains (Hungary). In: Lobitzer, H., Császár, G., Daurer, A. (Eds.), *Jubiläumsschrift 20 Jahre Geologische Zusammenarbeit Österreich-Ungarn* (Geologische Bund, vol. 2, pp. 145–207).
- Darder, B., 1945. Estudio geológico del sur de la Provincia de Valencia y norte de la de Alicante. *Boletín Geológico y Minero* 57, 59–837. España.
- de Gea, G.A., Castro, J.M., Company, M., O'Dogherty, L., Sandoval, J., Quijano, M.L., Sequero, C., Froehner, S., Aguado, R., 2024. New Evidence for an Episode of Accelerated Environmental Change in the Late Barremian: Geochemical and Paleontological Records from the Subbetic Basin (Western Tethys). *Geosciences* 14 (7), 187. <https://doi.org/10.3390/GEOSCIENCES14070187>, 2024, Vol. 14, Page 187.
- Del Viscio, G., Frijia, G., Posenato, R., Singh, P., Lehrmann, D.J., Payne, J.L., Al-Ramadan, K., Struck, U., Jochum, K.P., Morsilli, M., 2021. Proliferation of Chondrodonta as a proxy of environmental instability at the onset of OAE1a: Insights from shallow-water limestones of the Apulia Carbonate Platform. *Sedimentology* 68 (7), 3191–3227. <https://doi.org/10.1111/SED.12887>.
- Demico, R.V., Hardie, L.A., 1995. Sedimentary Structures and Early Diagenetic Features of Shallow Marine Carbonate Deposits. <https://api.semanticscholar.org/CorpusID:127070495>.
- Dunham, R.J., 1962. Classification of Carbonate Rocks According to Depositional Texture. In: Ham, W.E. (Ed.), *AAPG Memoir 1. Classification of Carbonate Rocks - A Symposium*. AAPG (American Association of Petroleum Geologists, pp. 108–121).
- Eberli, G.P., Ginsburg, R.N., 1989. Cenozoic Progradation of Northwestern Great Bahama Bank, a Record of Lateral Platform Growth and Sea-Level Fluctuations. *Controls on Carbonate Platform and Basin Development* 339–351. <https://doi.org/10.2110/PEC.89.44.0339>.
- Einsle, G., Ricken, W., Seilacher, A., 1991. Cycles and Events in Stratigraphy. <https://api.semanticscholar.org/CorpusID:128437866>.
- Erick, M., 1995. Cyclostratigraphy of Middle Devonian carbonates of the eastern Great Basin. *Journal of Sedimentary Research* 65 (1b), 61–79. <https://doi.org/10.1306/D42681E4-2B26-11D7-8648000102C1865D>.
- Embry, A.F., Klovan, J.E., 1971. A LATE DEVONIAN REEF TRACT ON NORTHEASTERN BANKS ISLAND, N.W.T. *Bulletin of Canadian Petroleum Geology* 19 (4), 730–781. <https://doi.org/10.35767/JSCPCBULL.19.4.730>.
- Embry, J.C., Vennin, E., Van Buchem, F.S.P., Schroeder, R., Pierre, C., Aurell, M., 2010. Sequence stratigraphy and carbon isotope stratigraphy of an Aptian mixed carbonate-siliciclastic platform to basin transition (Galve sub-basin, NE Spain). *Geological Society - Special Publications* 329, 113–143. <https://doi.org/10.1144/SP329.6>.
- Enos, P., Moore, C., 1983. Fore-reef slope environments. In: *Carbonate depositional environments*. AAPG Memoir, vol. 33. American Association of Petroleum Geologists, pp. 507–537.
- Erba, E., Duncan, R.A., Bottini, C., Tiraboschi, D., Weissert, H., Jenkyns, H.C., Malinverno, A., 2015. Environmental consequences of Ontong Java Plateau and Kerguelen Plateau volcanism. *Special Papers - Geological Society of America* 511 (15), 271–303. <https://doi.org/10.1130/2015.2511>.
- Evans, I., Kendall, C.C.G., Butler, J.C., 1977. Genesis of Liassic Shallow and Deep Water Rhythms Central High Atlas Mountains, Morocco. *Journal of Sedimentary Research* 47, 120–128. <https://api.semanticscholar.org/CorpusID:131501020>.
- Fallot, P., 1943. L'Urgonien de la Sierra Mariola (province d'Alicante). *C.R.Acad.Sci.-Paris*. Gauthier-Villars 216, 71–72.
- Fallot, P., 1948. Les Cordillères bétiques. *Estudios Geológicos* 8, 83–172.
- Flügel, E., 2010. *Microfacies of Carbonate Rocks: Analysis, Interpretation and Application*. Springer-Verlag Berlin Heidelberg, p. 976.
- Föllmi, K.B., Godet, A., Bodin, S., Linder, P., 2006. Interactions between environmental change and shallow water carbonate buildup along the northern Tethyan margin and their impact on the Early Cretaceous carbon isotope record. *Paleoceanography* 21 (4). <https://doi.org/10.1029/2006PA001313>.
- Föllmi, K.B., Weissert, H., Bisping, M., Funk, H., 1994. Phosphogenesis, carbon-isotope stratigraphy, and carbonate-platform evolution along the Lower Cretaceous northern Tethyan margin. *GSA Bulletin* 106 (6), 729–746. [https://doi.org/10.1130/0016-7606\(1994\)106<0729:PCISAC>2.3.CO;2](https://doi.org/10.1130/0016-7606(1994)106<0729:PCISAC>2.3.CO;2).
- Fragoso, D.G.C., Gabaglia, G.P.R., Magalhães, A.J.C., Dos Santos Scherer, C.M., 2021. Cyclicity and hierarchy in sequence stratigraphy: an integrated approach. *Brazilian Journal of Genetics* 51 (2), e20200106. <https://doi.org/10.1590/2317-4889202120200106>.
- Frau, C., Pictet, A., Spangenberg, J.E., Masse, J.-P., Tendil, A.J.-B., Lanteaume, C., 2017. New insights on the age of the post-Urgonian marly cover of the Apt region (Vaucluse, SE France) and its implications on the demise of the North Provence carbonate platform. *Sedimentary Geology* 359, 44–61.
- Funk, H., Föllmi, K.B., Mohr, H., 1993. Evolution of the Tithonian-Aptian carbonate platform along the northern Tethyan margin, eastern Helvetic Alps. In: *Cretaceous carbonate platforms*.
- García-Garnica, E.M., Pérez-Cruz, L., 2022. Hyperthermal events recorded in the Palaeogene carbonate sequence of southern Gulf of Mexico—Santa Elena borehole, Yucatan Peninsula. *Geological Journal* 57 (1), 99–113. <https://doi.org/10.1002/GJ.4285>.
- García Hernández, M., Castro Jiménez, J.M., Nieto Albert, L.M., 2003. La transgresión Aptiense en la Sierra de Segura (Zona Prebética, provincia de Jaén). *Geogaceta* 33, 127–130. ISSN 0213-683X, N.º. 33, 2002, Págs. 127-130. <https://dialnet.unirioja.es/servlet/articulo?codigo=7461383&info=resumen&idioma=ENG>.
- García-Hernández, M., Castro, J.M., Nieto, L.M., 2001. Los carbonatos del Cretácico Inferior del Prebético de la Sierra de Segura. In: Ruiz Ortiz, P., Molina, J., Nieto, L.M., Castro, J. (Eds.), *Itinerarios geológicos por el mesozoico de la provincia de Jaén*. Departamento de Geología, Universidad de Jaén, pp. 63–91.
- García-Penas, A., Aurell, M., Zamora, S., 2024. Sedimentary evolution and distribution of benthic fauna of an Aptian protected bay (Oliete Subbasin, Spain). *Sedimentary Geology* 461, 106577. <https://doi.org/10.1016/J.SEDGEO.2023.106577>.
- Giannetti, A., Monaco, P., Corbí, H., Soria, J.M., 2014. Integrated taphonomy in an open-marine platform: The Lower Cretaceous of Sierra Helada (Betic Cordillera, SE Spain). *Cretaceous Research* 51, 274–284. <https://doi.org/10.1016/j.cretres.2014.07.001>.
- Gili, E., Götz, S., 2018. Treatise Online no. 103: Part N, Volume 2, Chapter 26B: Paleocology of rudists. <https://doi.org/10.17161/to.v0i0.7183>.
- Gili, E., Skelton, P.W., Bover-Arnal, T., Salas, R., Obrador, A., Fenerci-Masse, M., 2016. Depositional biofacies model for post-OAE1a Aptian carbonate platforms of the western Maestrat Basin (Iberian Chain, Spain). *Palaeogeography, Palaeoclimatology, Palaeoecology* 453, 101–114. <https://doi.org/10.1016/J.PALAEO.2016.03.029>.
- Godet, A., Föllmi, K.B., Stille, P., Bodin, S., Matera, V., Adatte, T., 2011. Reconciling strontium-isotope and K-Ar ages with biostratigraphy: The case of the Urganian platform, Early Cretaceous of the Jura Mountains, Western Switzerland. *Swiss Journal of Geosciences* 104 (1), 147–160. <https://doi.org/10.1007/S00015-011-0053-5/TABLES/3>.
- Goldhammer, R.K., Oswald, E.J., Dunn, P.A., Franseen, E.K., Watney, W.L., 1991. Hierarchy of stratigraphic forcing: Example from Middle Pennsylvanian shelf carbonates of the Paradox Basin. *Kansas Geological Survey Bulletin* 233, 361–413.
- Graciansky, P.-C. de, Hardenbol, J., Jacquin, T., Vail, P.R., 1999. Mesozoic and Cenozoic Sequence Stratigraphy of European Basins. Mesozoic and Cenozoic Sequence Stratigraphy of European Basins. <https://doi.org/10.2110/PEC.98.02>.
- Gradstein, Ogg, F.M., George, J., Schmitz, M.D., Ogg, G.M., 2020. *Geologic time scale 2020*. Amsterdam: Elsevier.
- Granier, B., 1994. Early Valanginian unconformities in Central Atlantic and Western Mediterranean areas. *Geologie Méditerranéenne* 21 (3), 81–85. <https://doi.org/10.3406/GEOLM.1994.1532>.
- Granier, B., Perthuisot, V., 2009. Discussion of: Development of carbonate platforms on an extensional (rifted) margin: the Valanginian–Albian record of the Prebetic of Alicante (SE Spain), by J.M. Castro et al. *Cretaceous Research* 29. <https://doi.org/10.1016/j.cretres.2009.03.002> (2008), 848–860. *Cretaceous Research*, 30(4), 1019–1026.
- Granier, B., Virgone, A., Busnardo, R., Bulot, L.G., 1995. Des calpionelles dans l'Hauteriviens supérieur. Découverte exceptionnelle à Busot (Alicante, Espagne). *Comptes Rendus de l'Académie Des Sciences. Série 2. Sciences de La Terre et Des Planètes* 321 (12), 1179–1186.
- Graziano, R., 2000. The Aptian–Albian of the Apulia Carbonate Platform (Gargano Promontory, southern Italy): evidence of palaeoenvironmental and tectonic controls on the stratigraphic architecture of the platform margin. *Cretaceous Research* 21 (1), 107–126. <https://doi.org/10.1006/CRES.2000.0201>.
- Graziano, R., Raspini, A., 2018. High-resolution chronostratigraphy of palaeoecologic and isotopic changes in shallow-marine carbonates: Deciphering the completeness of the Aptian record in the Apennine carbonate platform (southern Italy). *Cretaceous Research* 86, 97–128. <https://doi.org/10.1016/J.CRETRES.2017.12.008>.
- Grotzinger, J.P., 1986. Cyclicity and paleoenvironmental dynamics Rocknest platform, northwest Canada. *Geological Society of America Bulletin* 97 (10), 1208–1231. [https://doi.org/10.1130/0016-7606\(1986\)97<1208:CAPDRP>2.0.CO;2](https://doi.org/10.1130/0016-7606(1986)97<1208:CAPDRP>2.0.CO;2).
- Hallock, P., 1985. Why Are Larger Foraminifera Large? *Paleobiology* 11 (2), 195. <https://doi.org/10.1017/S0094837300011507>.
- Hardenbol, J., Thierry, J., Farley, M.B., Jacquin, T., de Graciansky, P.C., Vail, P.R., 1998. Mesozoic and Cenozoic sequence chronostratigraphic chart. In: 60th ed. de Graciansky, P.C., Hardenbol, J., Jacquin, T., Vail, P.R. (Eds.), *Mesozoic and Cenozoic sequence stratigraphy of European basins*. Special Publication. Society for Sedimentary Geology.
- Hardie, L.A., Bosellini, A., Goldhammer, R.K., 1986. Repeated subaerial exposure of subtidal carbonate platforms, Triassic, northern Italy: Evidence for high frequency sea level oscillations on a 10<sup>4</sup> year scale. *Paleoceanography* 1 (4), 447–457. <https://doi.org/10.1029/PA0011004p00447>.
- Hay, W.W., DeConto, R.M., de Boer, P., Flügel, S., Song, Y., Stepashko, A., 2019. Possible solutions to several enigmas of Cretaceous climate. *International Journal of Earth Sciences* 108 (2), 587–620. <https://doi.org/10.1007/s00531-018-1670-2>.
- Heimhofer, U., Adatte, T., Hochuli, P.A., Burla, S., Weissert, H., 2008. Coastal sediments from the Algarve: Low-latitude climate archive for the Aptian–Albian. *International Journal of Earth Sciences* 97 (4), 785–797. <https://doi.org/10.1007/S00531-007-0186-Y>.
- Hilgen, F., Zeeden, C., Laskar, J., 2020. Paleoclimate records reveal elusive ~200-kyr eccentricity cycle for the first time. *Global and Planetary Change* 194, 103296. <https://doi.org/10.1016/J.GLOPLACHA.2020.103296>.
- Hottinger, L., 1982. Larger foraminifera, giant cells with a historical background. *Naturwissenschaften* 69 (8), 361–371. <https://doi.org/10.1007/BF00396687/METRICS>.

- Huck, S., Heimhofer, U., 2015. Improving shallow-water carbonate chemostratigraphy by means of rudist bivalve sclerochemistry. *Geochemistry, Geophysics, Geosystems* 16 (9), 3111–3128. <https://doi.org/10.1002/2015GC005988>.
- Huck, S., Heimhofer, U., Rameil, N., Bodin, S., Immenhauser, A., 2011. Strontium and carbon-isotope chronostratigraphy of Barremian–Aptian shallow-water carbonates: Northern Tethyan platform drowning predates OAE 1a. *Earth and Planetary Science Letters* 304 (3–4), 547–558. <https://doi.org/10.1016/j.epsl.2011.02.031>.
- Immenhauser, A., Hillgärtner, H., Sattler, U., Bertotti, G., Schoepfer, P., Homewood, P., Vahrenkamp, V., Steuber, T., Masse, J.P., Droste, H., Taal-van Koppen, J., van der Kooij, B., van Bentum, E., Verwer, K., Strating, E.H., Swinkels, W., Peters, J., Immenhauser-Pothast, I., Al Maskery, S., 2004. Barremian-lower Aptian Qishn Formation, Haushi-Huqf area, Oman: a new outcrop analogue for the Kharaib/Shu'aiba reservoirs. *GeoArabia* 9 (1), 153–194. <https://doi.org/10.2113/GEOARABIA0901153>.
- Immenhauser, A., Scott, R.W., 2002. An estimate of Albian sea-level amplitudes and its implication for the duration of stratigraphic hiatuses. *Sedimentary Geology* 152 (1–2), 19–28. [https://doi.org/10.1016/S0037-0738\(02\)00260-9](https://doi.org/10.1016/S0037-0738(02)00260-9).
- James, N.P., Dalrymple, R.W., 2010. Facies Models 4. In: *St. John's Geological Association of Canada, Newfoundland. Geological Association of Canada*.
- James, N.P., Mountjoy, E.W., 1983. Shelf-slope break in fossil carbonate platforms: an overview. *SEPM (Society for Sedimentary Geology), Special Publication* 33, 189–206.
- Jarvis, I., Lignum, J.S., Grcke, D.R., Jenkyns, H.C., Pearce, M.A., 2011. Black shale deposition, atmospheric CO<sub>2</sub> drawdown, and cooling during the Cenomanian-Turonian Oceanic Anoxic Event. *Paleoceanography* 26 (3). <https://doi.org/10.1029/2010PA002081>.
- Jenkyns, H.C., 1995. Carbon-isotope stratigraphy and paleoceanographic significance of the Lower Cretaceous shallow-water carbonates of Resolution Guyot, Mid-Pacific Mountains. In: *Proceedings of the Ocean Drilling Program, Scientific Results*, vol. 143, pp. 99–104.
- Jenkyns, H.C., 2010. Geochemistry of oceanic anoxic events. *Geochemistry, Geophysics, Geosystems* 11 (3). <https://doi.org/10.1029/2009GC002788>.
- Kidwell, S.M., Bosence, D.W.J., Allison, P.A., Briggs, D.E.G., others, 1991. Taphonomy and time-averaging of marine shelly faunas. *Taphonomy: Releasing the Data Locked in the Fossil Record* 9, 115–209.
- Lechler, M., Pogge von Strandmann, P.A.E., Jenkyns, H.C., Prosser, G., Parente, M., 2015. Lithium-isotope evidence for enhanced silicate weathering during OAE 1a (Early Aptian Selli event). *Earth and Planetary Science Letters* 432, 210–222. <https://doi.org/10.1016/j.epsl.2015.09.052>.
- Leckie, R.M., Bralower, T.J., Cashman, R., 2002. Oceanic anoxic events and plankton evolution: Biotic response to tectonic forcing during the mid-Cretaceous. *Paleoceanography* 17 (3), 13–13–29. <https://doi.org/10.1029/2001PA000623>.
- Lorenzen, J., Kuhn, W., Holbourn, A., Flögel, S., Moullade, M., Tronchetti, G., 2013. A new sediment core from the Bedoulian (Lower Aptian) stratotype at Roquefort-La Bédoule, SE France. *Cretaceous Research* 39, 6–16. <https://doi.org/10.1016/j.cretres.2012.03.019>.
- Löser, H., 2001. Le site de Vallières (département de l'Aube, France): résultats préliminaires sur des coraux de l'Hauterivien inférieur (Crétacé). *Bulletin de l'année...-Association Géologique Aubeoise* 22, 39–53.
- Machel, H.G., 2004. Concepts and models of dolomitization: A critical reappraisal. *Geological Society - Special Publications* 235, 7–63. <https://doi.org/10.1144/GSL.SP.2004.235.01.02>.
- Malchus, N., Pons, J.M., Salas, R., 1995. Rudist distribution in the lower Aptian shallow platform of La Mola de Xert, eastern Iberian range, NE Spain. *Revista Mexicana de Ciencias Geológicas* 12 (2), 224–235. <https://portalrecerca.uab.cat/en/publicacions/rudist-distribution-in-the-lower-aptian-shallow-platform-of-la-mo>.
- Martín-Chivelet, J., López-Gómez, J., Aguado, R., Arias, C., Arribas, J., Arribas, M.E., Aurell, M., Bádenas, B., Benito, M.L., Bover-Arnal, T., Casas-Sainz, A., Castro, J.M., Coruña, F., de Gea, G.A., Fornós, J.J., Fregenal-Martínez, M., García-Senz, J., Garófano, D., Gelabert, B., Vilas, L., 2019. The Late Jurassic–Early Cretaceous Rifting - A timescale for climate change during the early Aptian Anoxic Event (OAE 1a) and the late Aptian. *Global and Planetary Change* 233, 104361. <https://doi.org/10.1016/j.gloplacha.2024.104361>.
- Martínez-Rodríguez, R., Castro, J.M., De, G.A., Guillén, G., Nieto, L.M., Reolid, M., Ruiz-Ortiz, P.A., 2018. Facies analysis and stratigraphy of a lower Aptian carbonate platform section (Prebetic, Alicante, Spain) Estratigrafía y análisis de facies de una sección de una plataforma de carbonatos del Aptiense inferior (Prebético, Alicante, España). *Geogaceta* 64, 31–34. [www.geogaceta.com](http://www.geogaceta.com).
- Martínez-Rodríguez, R., Nieto, L.M., Castro, J.M., de Gea, G.A., Ruiz-Ortiz, P.A., Molina, J.M., Skelton, P.W., 2023. Progradation of a shallow carbonate platform developed on a fault-block in the Western Tethys (lower Aptian, Sierra de Bedmar-Jódar, Prebetic of Jaén, Spain). *Facies* 69 (2), 1–18. <https://doi.org/10.1007/S10347-023-00664-9/FIGURES/9>.
- Martínez-Rodríguez, R., Selby, D., Castro, J.M., de Gea, G.A., Nieto, L.M., Ruiz-Ortiz, P.A., 2021. Tracking magmatism and oceanic change through the early Aptian Anoxic Event (OAE 1a) to the late Aptian: Insights from osmium isotopes from the westernmost Tethys (SE Spain) Cau Core. *Global and Planetary Change* 207, 103652. <https://doi.org/10.1016/j.gloplacha.2021.103652>.
- Masse, J.P., Bellion, Y., Benkheil, J., Ricou, L.E., Dercourt, J., Guiraud, R., 1993. Early Aptian (114 to 111 Ma). In: *Dercourt, J., Ricou, L.E., Vrielynck, B. (Eds.), Atlas, Tethys, palaeoenvironmental maps*. Gauthier-Villars, Paris, pp. 135–152.
- Menegatti, A.P., Weissert, H., Brown, R.S., Tyson, R.V., Farrimond, P., Strasser, A., Caron, M., 1998. High-resolution  $\delta^{13}\text{C}$  stratigraphy through the Early Aptian "Livello Selli" of the Alpine tethys. *Paleoceanography* 13 (5), 530–545. <https://doi.org/10.1029/98PA01793>.
- Millán, M.I., Weissert, H.J., Owen, H., Fernández-Mendiola, P.A., García-Mondéjar, J., 2011. The Madotz Urganian platform (Aralar, northern Spain): Paleoclimatic changes in response to Early Aptian global environmental events. *Paleoceanography, Palaeoclimatology, Palaeoecology* 312 (1–2), 167–180. <https://doi.org/10.1016/j.palaeo.2011.10.005>.
- Najarro, M., Rosales, I., Martín-Chivelet, J., 2011a. Major palaeoenvironmental perturbation in an Early Aptian carbonate platform: Prelude of the Oceanic Anoxic Event 1a? *Sedimentary Geology* 235 (1–2), 50–71. <https://doi.org/10.1016/j.sedgelo.2010.03.011>.
- Najarro, M., Rosales, I., Moreno-Bedmar, J.A., de Gea, G.A., Barrón, E., Company, M., Delanoy, G., 2011b. High-resolution chemo- and biostratigraphic records of the Early Aptian oceanic anoxic event in Cantabria (N Spain): Palaeoceanographic and palaeoclimatic implications. *Paleoceanography, Palaeoclimatology, Palaeoecology* 299 (1–2), 137–158. <https://doi.org/10.1016/j.palaeo.2010.10.042>.
- Nicklès, R., 1891. *Recherches géologiques sur les terrains secondaires et tertiaires de la province d'Alicante et du Sud de la province de Valence*, vol. 1. Impr. L. Danel.
- Olierook, H.K.H., Jourdan, F., Merle, R.E., 2019. Age of the Barremian–Aptian boundary and onset of the Cretaceous Normal Superchron. *Earth-Science Reviews* 197, 102906. <https://doi.org/10.1016/j.earscirev.2019.102906>.
- Parente, M., Frijia, G., Di Lucia, M., Jenkyns, H.C., Woodfine, R.G., Baroncini, F., 2008. Stepwise extinction of larger foraminifers at the Cenomanian-Turonian boundary: A shallow-water perspective on nutrient fluctuations during Oceanic Anoxic Event 2 (Bonarelli Event). *Geology* 36 (9), 715–718. <https://doi.org/10.1130/G24893A.1>.
- Pasquier, J.B., Strasser, A., 1997. Platform-to-basin correlation by high-resolution sequence stratigraphy and cyclostratigraphy (Berriasi, Switzerland and France). *Sedimentology* 44 (6), 1071–1092. <https://doi.org/10.1046/j.1365-3091.1997.D01-62.X>.
- Pemberton, S.G., MacEachern, J.A., Dashtgard, S.E., Bann, K.L., Gingras, M.K., Zonneveld, J.P., 2012. Shorefaces. *Developments in Sedimentology* 64, 563–603. <https://doi.org/10.1016/B978-0-444-53813-0.00019-8>.
- Photiadis, A., Pomoni-Papaioannou, F.A., Kostopoulou, V., 2010. Correlation of Late Triassic and Early Jurassic lifer-type carbonates from the Peloponnese Peninsula, Greece. *Bulletin of the Geological Society of Greece* 43 (2), 726–736. <https://doi.org/10.12681/bgsg.11235>.
- Pittet, B., Van Buchem, F.S.P., Hillgärtner, H., Razin, P., Grötsch, J., Droste, H., 2002. Ecological succession, palaeoenvironmental change, and depositional sequences of Barremian–Aptian shallow-water carbonates in northern Oman. *Sedimentology* 49 (3), 555–583. <https://doi.org/10.1046/j.1365-3091.2002.00460.x>.
- Posenato, R., Bassi, D., Trecalli, A., Parente, M., 2018. Taphonomy and evolution of Lower Jurassic lithiotid bivalve accumulations in the Apennine Carbonate Platform (southern Italy). *Paleoceanography, Palaeoclimatology, Palaeoecology* 489, 261–271. <https://doi.org/10.1016/j.palaeo.2017.10.017>.
- Pratt, B.R., James, N.P., 1986. The St George Group (Lower Ordovician) of western Newfoundland: tidal flat island model for carbonate sedimentation in shallow epicritic seas. *Sedimentology* 33 (3), 313–343. <https://doi.org/10.1111/j.1365-3091.1986.tb00540.x>.
- Purdy, E.G., Winterer, E.L., 2001. Origin of atoll lagoons. *GSA Bulletin* 113 (7), 837–854. [https://doi.org/10.1130/0016-7606\(2001\)113<0837:OOAL>2.0.CO;2](https://doi.org/10.1130/0016-7606(2001)113<0837:OOAL>2.0.CO;2).
- Rameil, N., Immenhauser, A., Warrlich, G., Hillgärtner, H., Droste, H.J., 2010. Morphological patterns of Aptian Lithocodium–Bacinnella geobodies: relation to environment and scale. *Sedimentology* 57 (3), 883–911. <https://doi.org/10.1111/j.1365-3091.2009.01124.x>.
- Reijmer, J.J.G., 2021. Marine carbonate factories: Review and update. *Sedimentology* 68 (5), 1729–1796. <https://doi.org/10.1111/sed.12878>.
- Reijmer, J., Schlager, W., Droxler, A., 1988. Site 632: Pliocene-Pleistocene sedimentation cycles in Bahamian basin. In: *Austin, J., Schlager, W., Comet, P. (Eds.), Proc. scientific results, ODP, Leg 101, Bahamas*, pp. 213–220.
- Rosales, I., 1999. Controls on carbonate-platform evolution on active fault blocks: the Lower Cretaceous Castro Urdiales Platform (Aptian-Albian, northern Spain). *Journal of Sedimentary Research* 69 (2), 447–465. <https://doi.org/10.2110/j.sed.69.447>.
- Rosen, B.R., Aillud, G.S., Bosellini, F., Clack, N.J., Insalaco, E., Valldeperas, F.X., Wilson, M.E.J., 2000. Platy coral assemblages. 200 million years of functional stability in response to the limiting effects of light and turbidity. *9th International Coral-Reef-Symposium*, pp. 255–264.
- Ruddiman, W., 2014. *Earth's climate: past and future*, third ed. Macmillan Learning.
- Ruiz Ortiz, P.A., 2010. Contribución al conocimiento de las zonas externas de la Cordillera Bética a lo largo de 30 años de investigación geológica: Discurso de Ingreso en el Instituto de Estudios Giennenses. *Diputación Provincial de Jaén*, 0–96.

- Ruiz-Ortiz, P.A., Castro, J., 1998. Carbonate depositional sequences in shallow to hemipelagic platform deposits; Aptian, Prebetic of Alicante (SE Spain). *Bulletin de la Societe Geologique de France* 169 (1), 21–33.
- Sandulli, R., Raspini, A., 2004. Regional to global correlation of lower Cretaceous (Hauterivian–Barremian) shallow-water carbonates of the southern Apennines (Italy) and Dinarides (Montenegro), southern Tethyan Margin. *Sedimentary Geology* 165 (1–2), 117–153. <https://doi.org/10.1016/j.SEDGEO.2003.11.014>.
- Satterley, A.K., 1996. The interpretation of cyclic successions of the Middle and Upper Triassic of the Northern and Southern Alps. *Earth-Science Reviews* 40 (3–4), 181–207. [https://doi.org/10.1016/0012-8252\(95\)00063-1](https://doi.org/10.1016/0012-8252(95)00063-1).
- Schlager, W., 1992. Sedimentology and sequence stratigraphy of reefs and carbonate platforms. Continuing Education Course Note Series 34. American Association of Petroleum Geologists. <https://www.osti.gov/biblio/5124424>.
- Schlager, W., 2003. Benthic carbonate factories of the Phanerozoic. *International Journal of Earth Sciences* 92 (4), 445–464. <https://doi.org/10.1007/S00531-003-0327-X/METRICS>.
- Schlager, W., 2005. Carbonate Sedimentology and Sequence Stratigraphy. SEPM Society for Sedimentary Geology. <https://doi.org/10.2110/csp.05.08>.
- Schlager, W., Philip, J., 1990. Cretaceous Carbonate Platforms. *Cretaceous Resources, Events and Rhythms* 173–195. [https://doi.org/10.1007/978-94-015-6861-6\\_9](https://doi.org/10.1007/978-94-015-6861-6_9).
- Schlager, W., Reijmer, J.J.G., Droxler, A., 1994. Highstand shedding of carbonate platforms. *Journal of Sedimentary Research* 64 (3b), 270–281. <https://doi.org/10.1306/D4267FAA-2B26-11D7-8648000102C1865D>.
- Shahzad, K., Betzler, C., Qayyum, F., 2019. Controls on the Paleogene carbonate platform growth under greenhouse climate conditions (Offshore Indus Basin). *Marine and Petroleum Geology* 101, 519–539. <https://doi.org/10.1016/j.marpetgeo.2018.12.025>.
- Sibley, D.F., Gregg, J.M., 1987. Classification of dolomite rock textures. *Journal of Sedimentary Research* 57 (6), 967–975. <https://doi.org/10.1306/212F8CBA-2B24-11D7-8648000102C1865D>.
- Simo, J.A.T., Scott, R.W., Masse, J.-P., 1993. Cretaceous Carbonate Platforms: An Overview: Chapter 1. In: Simo, J., Scott, R., Masse, J. (Eds.), *Cretaceous Carbonate Platforms - An Overview*. AAPG Special Volumes, pp. 1–14.
- Skelton, P., Spicer, R.A., Kelley, S.P., Gilmour, I., 2003a. In: Skelton, P.W. (Ed.), *The Cretaceous World*. Cambridge University Press for The Open University.
- Skelton, P.W., Castro, J.M., Ruiz-Ortiz, P.A., 2019. Aptian carbonate platform development in the Southern Iberian Palaeomargin (Prebetic of Alicante, SE Spain). *BSGF - Earth Sciences Bulletin* 190, 3. <https://doi.org/10.1051/BSGF/2019001>.
- Skelton, P.W., Gili, E., 2012. Rudists and carbonate platforms in the Aptian: a case study on biotic interactions with ocean chemistry and climate. *Sedimentology* 59 (1), 81–117. <https://doi.org/10.1111/j.1365-3091.2011.01292.x>.
- Skelton, P.W., Gili Folch, E., Vicens Batet, E., Obrador Tuduri, A., López Sanjaume, G., 2003b. Revised lithostratigraphy of the Upper Cretaceous (Santonian) carbonate platform succession on the northern flank of Sant Corneli, southern Central Pyrenees. *Journal of Iberian Geology: An International Publication of Earth Sciences* 29, 73–88. ISSN-e 1886-7995, ISSN 1698-6180, Nº. 29, 2003 (*Ejemplar Dedicado a: Nuevas Perspectivas Sobre El Cretácico de España*), Págs. 73–88.
- Stein, M., Arnaud-Vanneau, A., Adatte, T., Fleitmann, D., Spangeberg, J.E., Föllmi, K.B., 2012. Palaeoenvironmental and palaeoecological change on the northern Tethyan carbonate platform during the Late Barremian to earliest Aptian. *Sedimentology* 59 (3), 939–963. <https://doi.org/10.1111/j.1365-3091.2011.01286.x>.
- Strasser, A., 2015. Hiatuses and condensation: an estimation of time lost on a shallow carbonate platform. *The Depositional Record* 1 (2), 91–117. <https://doi.org/10.1002/DEP2.9>.
- Strasser, A., 2018. Cyclostratigraphy of Shallow–Marine Carbonates – Limitations and Opportunities, vol. 3, pp. 151–187. <https://doi.org/10.1016/BS.SATS.2018.07.001>.
- Strasser, A., Pittet, B., Hillgärtner, H., Pasquier, J.B., 1999. Depositional sequences in shallow carbonate-dominated sedimentary systems: concepts for a high-resolution analysis. *Sedimentary Geology* 128 (3–4), 201–221. [https://doi.org/10.1016/S0037-0738\(99\)00070-6](https://doi.org/10.1016/S0037-0738(99)00070-6).
- Tejada, M.L.G., Suzuki, K., Kuroda, J., Coccioni, R., Mahoney, J.J., Ohkouchi, N., Sakamoto, T., Tatsumi, Y., 2009. Ontong Java Plateau eruption as a trigger for the early Aptian oceanic anoxic event. *Geology* 37 (9), 855–858. <https://doi.org/10.1130/G25763A.1>.
- Tomás, S., Löser, H., Salas, R., 2008. Low-light and nutrient-rich coral assemblages in an Upper Aptian carbonate platform of the southern Maestrat Basin (Iberian Chain, eastern Spain). *Cretaceous Research* 29 (3), 509–534. <https://doi.org/10.1016/j.CRETRES.2007.09.001>.
- Tresch, J., Strasser, A., 2011. Allogenic and autogenic processes combined in the formation of shallow-water carbonate sequences (Middle Berriasian, Swiss and French Jura Mountains). *Swiss Journal of Geosciences* 104 (2), 299–322. <https://doi.org/10.1007/s00015-011-0064-2>.
- Tucker, M.E., Wright, V.P., 1990. *Carbonate sedimentology*. Blackwell.
- van Buchem, F.S.P., Pittet, B., Hillgärtner, H., Grötsch, J., Mansouri, A. I. Al, Billing, I., Droste, H.J., Oterdoom, W.H., van Steenwinkel, M., 2002. High-resolution Sequence Stratigraphic Architecture of Barremian/Aptian Carbonate Systems in Northern Oman and the United Arab Emirates (Kharaib and Shu'aiba Formations). *GeoArabia* 7 (3), 461–500. <https://api.semanticscholar.org/CorpusID:201106847>.
- Van Wagoner, J.C., Posamentier, H.W., Mitchum, R.M., Vail, P.R., Sarg, J.F., Loutit, J.S., Hardenbol, J., 1998. An overview of the fundamentals of sequence stratigraphy and key definitions. In: Wilgus, C.K., Hastings, B.S., Kendall, C.G.S.T.C., Posamentier, H.W., Ross, C.A., Van Wagoner, J.C. (Eds.), *Sea-level changes: an integrated approach: Vol. Special Pu. Society of Economic Paleontologists and Mineralogists*, pp. 38–45.
- Vera, J., 2004. Cordillera Bética y Baleares. In: Vera, J. (Ed.), *Geología de España*. SGE-IGME, p. 890.
- Vera, J.A., 2001. Evolution of the Southern Iberian Continental Margin. In: Ziegler, P., Cavazza, W., Robertson, A.F.H., Craquin-Soleau, S. (Eds.), *Peri-tethys Memoir 6: Peri-Tethyan Rift-Wrench Basins and Passive Margins*, vol. 186. Mémoires du Muséum National d'Histoire naturelle, pp. 109–143.
- Vilas, L., Castro, J., Martín-Chivelet, J., Company, M., Ruiz-Ortiz, P., Arias, C., Estévez, A., 2004. El Prebético del sector oriental. In: Vera, J. (Ed.), *Geología de España*. SGE, pp. 361–363.
- Vilas, L., Masse, J., Arias, C., 1993. Aptian mixed terrigenous and carbonate platforms from Iberic and Prebetic regions. In: Simo, J., Scott, R., Masse, J. (Eds.), *Cretaceous carbonate platforms - AAPG Memoir 56*. American Association of Petroleum Geologists, pp. 243–253.
- Vilas, L., Masse, J.P., Arias, C., 1995. Orbitolina episodes in carbonate platform evolution: the early Aptian model from SE Spain. *Palaeogeography, Palaeoclimatology, Palaeoecology* 119 (1), 35–45. [https://doi.org/10.1016/0031-0182\(95\)00058-5](https://doi.org/10.1016/0031-0182(95)00058-5).
- Wilkinson, B.H., Drummond, C.N., Rothman, E.D., Diedrich, N.W., 1997. Stratal Order in Peritidal Carbonate Sequences. *Journal of Sedimentary Research* 67, 1068–1082. <https://api.semanticscholar.org/CorpusID:130029551>.
- Wilmsen, M., 2000. Evolution and demise of a mid-Cretaceous carbonate shelf: the Altamira Limestones (Cenomanian) of northern Cantabria (Spain). *Sedimentary Geology* 133 (3–4), 195–226. [https://doi.org/10.1016/S0037-0738\(00\)00036-1](https://doi.org/10.1016/S0037-0738(00)00036-1).
- Wilson, J.L., 1975. *Carbonate Facies in Geologic History*. Springer-Verlag.
- Wissler, L., Funk, H., Weissert, H., 2003. Response of Early Cretaceous carbonate platforms to changes in atmospheric carbon dioxide levels. *Palaeogeography, Palaeoclimatology, Palaeoecology* 200 (1–4), 187–205. [https://doi.org/10.1016/S0031-0182\(03\)00450-4](https://doi.org/10.1016/S0031-0182(03)00450-4).
- Wissler, L., Weissert, H., Buonocunto, F.P., Ferreri, V., D'Argenio, B., 2004. Calibration of the Early Cretaceous Time Scale: A Combined Chemostratigraphic and Cyclostratigraphic Approach to the Barremian–Aptian Interval, Campania Apennines and Southern Alps (Italy). *Cyclostratigraphy: Approaches and Case Histories* 123–133. <https://doi.org/10.2110/PEC.04.81.0123>.
- Yilmaz, I.Ö., Altiner, D., 2007. Cyclostratigraphy and sequence boundaries of inner platform mixed carbonate–siliciclastic successions (Barremian–Aptian) (Zonguldak, NW Turkey). *Journal of Asian Earth Sciences* 30 (2), 253–270. <https://doi.org/10.1016/J.JSEAES.2006.08.008>.

## Appendix A. Supplementary data

Supplementary data to this article can be found online at <https://doi.org/10.1016/j.cretres.2024.106032>.